

1 **Exploring water cycle dynamics by sampling multiple**
2 **stable water isotope pools in a developed landscape of**
3 **Germany**

4
5 **N. Orlowski^{1,2}, P. Kraft¹, J. Pferdmenges¹ and L. Breuer^{1,3}**

6 [1]{Institute for Landscape Ecology and Resources Management (ILR), Research Centre for
7 BioSystems, Land Use and Nutrition (iFZ), Justus Liebig University Giessen, Giessen,
8 Germany}

9 [2]{Global Institute for Water Security, University of Saskatchewan, Saskatoon, Canada}

10 [3]{Centre for International Development and Environmental Research, Justus Liebig
11 University Giessen, Germany}

12 Correspondence to: N. Orlowski (Natalie.Orlowski@umwelt.uni-giessen.de)

13
14 **Abstract**

15 A dual stable water isotope ($\delta^2\text{H}$ and $\delta^{18}\text{O}$) study was conducted in the developed (managed)
16 landscape of the Schwingbach catchment (Germany). The two-year weekly to biweekly
17 measurements of precipitation, stream, and groundwater isotopes revealed that surface and
18 groundwater are isotopically disconnected from the annual precipitation cycle but showed
19 bidirectional interactions between each other. Apparently, snowmelt played a fundamental role
20 for groundwater recharge explaining the observed differences to precipitation δ -values.

21 A spatially distributed snapshot sampling of soil water isotopes in two soil depths at 52
22 sampling points across different land uses (arable land, forest, and grassland) revealed that top
23 soil isotopic signatures were similar to the precipitation input signal. Preferential water flow
24 paths occurred under forested soils explaining the isotopic similarities between top and subsoil
25 isotopic signatures. Due to human-impacted agricultural land use (tilling and compression) of
26 arable and grassland soils, water delivery to the deeper soil layers was reduced, resulting in
27 significant different isotopic signatures. However, the land use influence became less
28 pronounced with depth and soil water approached groundwater δ -values. Seasonally tracing

29 stable water isotopes through soil profiles showed that the influence of new percolating soil
30 water decreased with depth as no remarkable seasonality in soil isotopic signatures was obvious
31 at depth >0.9 m and constant values were observed through space and time. Since classic
32 isotope evaluation methods such as transfer function based mean transit time calculations did
33 not provide a good fit between the observed and calculated data, we established a hydrological
34 model to estimate spatially distributed groundwater ages and flow directions within the
35 Vollnkirchener Bach subcatchment. Our model revealed that complex age dynamics exist
36 within the subcatchment and that much of the runoff must have been stored for much longer than
37 event water (average water age is 16 years). Tracing stable water isotopes through the water
38 cycle in combination with our hydrological model was valuable for determining interactions
39 between different water cycle components and unravelling age dynamics within the study area.
40 This knowledge can further improve catchment specific process understanding of developed,
41 human-impacted landscapes.

42 **1 Introduction**

43 The application of stable water isotopes as natural tracers in combination with hydrodynamic
44 methods has been proven to be a valuable tool for studying the origin and formation of
45 recharged water as well as the interrelationship between surface water and groundwater
46 (Blasch and Bryson, 2007), partitioning evaporation and transpiration (Wang and Yakir,
47 2000), and mixing processes between various water sources (Clark and Fritz, 1997c).
48 Particularly in catchment hydrology, stable water isotopes play a major role since they can be
49 utilised for hydrograph separations (Buttle, 2006), to calculate the mean transit time (McGuire
50 and McDonnell, 2006), to investigate water flow paths (Barthold et al., 2011), or to improve
51 hydrological model simulations (Windhorst et al., 2014). However, most of our current
52 understanding is resulting from studies in forested catchments. Spatio-temporal studies of
53 stream water in developed, agricultural dominated, and managed catchments are less
54 abundant. This is partly caused by damped stream water isotopic signatures excluding
55 traditional hydrograph separations in low-relief catchments (Klaus et al., 2015). Unlike the
56 distinct watershed components found in steeper headwater counterparts, lowland areas often
57 exhibit a complex groundwater–surface water interaction (Klaus et al., 2015). Sklash and
58 Farvolden (1979) showed that groundwater plays an important role as a generating factor for
59 storm and snowmelt runoff processes. In many catchments, streamflow responds promptly to
60 rainfall inputs but variations in passive tracers such as water isotopes are often strongly
61 damped (Kirchner, 2003). This indicates that storm runoff in these catchments is dominated

62 mostly by “old water” (Buttle, 1994; Neal and Rosier, 1990; Sklash, 1990). However, not all
63 “old water” is the same (Kirchner, 2003). This catchment behaviour was described by
64 Kirchner (2003) as the old water paradox. Thus, there is evidence of complex age dynamics
65 within catchments and much of the runoff is stored in the catchment for much longer than
66 event water (Rinaldo et al., 2015). Still, some of the physical processes controlling the release
67 of “old water” from catchments are poorly understood, roughly modelled, and the observed
68 data do not suggest a common catchment behaviour (Botter et al., 2010). However, old water
69 paradox behaviour was observed in many catchments worldwide but it may have the strongest
70 effect in agriculturally managed catchments, where surprisingly only small changes in stream
71 chemistry have been observed (Hrachowitz et al., 2016).

72 Moreover, almost all European river systems were already substantially modified by humans
73 before river ecology research developed (Allan, 2004). Through changes in land use, land
74 cover, irrigation, and draining, agriculture has substantially modified the water cycle in terms
75 of both quality and quantity (Gordon et al., 2010) as well as hydrological functioning (Pierce et
76 al., 2012). Hrachowitz et al. (2016) recently stated the need for a stronger linkage between
77 catchment-scale hydrological and water quality communities. Further, McDonnell et al. (2007)
78 concluded that we need to figure out a way to embed landscape heterogeneity or the
79 consequence of the heterogeneity (i.e. of agricultural dominated and managed catchments) into
80 models as current generation catchment-scale hydrological and water quality models are poorly
81 linked (Hrachowitz et al., 2016).

82 One way to better understand catchment behaviour and the interaction among the various water
83 sources (surface, subsurface, and groundwater) and their variation in space and time is a detailed
84 knowledge about their isotopic composition. In principal, isotopic signatures of precipitation
85 are altered by temperature, amount (or rainout), continental, altitudinal, and seasonal effects.
86 Stream water isotopic signatures can reflect precipitation isotopic composition and moreover,
87 dependent on discharge variations be affected by seasonally variable contributions of different
88 water sources such as bidirectional water exchange with the groundwater body during baseflow,
89 or high event-water contributions during stormflow (Genereux and Hooper, 1998; Koeniger et
90 al., 2009). Precipitation falling on vegetated areas is partly intercepted by plants and re-
91 evaporated isotopically fractionated. The remaining throughfall infiltrates slower and can be
92 affected by evaporation resulting in an enrichment of heavy isotopes, particularly in the upper
93 soil layers (Gonfiantini et al., 1998; Kendall and Caldwell, 1998). In the soil, specific isotopic

94 profiles develop, characterized by an evaporative layer near the surface. The isotopic
95 enrichment decreases exponentially with depth, representing a balance between the upward
96 convective flux and the downward diffusion of the evaporative signature (Barnes and Allison,
97 1988). In humid and semi-humid areas, this exponential decrease is generally interrupted by the
98 precipitation isotopic signal. Hence, the combination of the evaporation effect and the
99 precipitation isotopic signature determine the isotope profile in the soil (Song et al., 2011).
100 Once soil water reaches the saturated zone, this isotope information is finally transferred to the
101 groundwater (Song et al., 2011). Soil water can therefore be seen as a link between precipitation
102 and groundwater, and the dynamics of isotopic composition in soil water are indicative of the
103 processes of precipitation infiltration, evaporation of soil water, and recharge to groundwater
104 (Blasch and Bryson, 2007; Song et al., 2011).

105 We started our research with results obtained through an earlier study in the managed
106 Schwingbach catchment that implied a high responsiveness of the system to precipitation inputs
107 indicated by very fast rises in discharge and groundwater head levels (Orlowski et al., 2014).
108 However, as there was only a negligible influence of the precipitation input signal on the stable
109 water isotopic composition in streams, our initial data set showed evidence for complex age
110 dynamics within the catchment. Nevertheless, a rapid flow response to a precipitation input may
111 also be mistaken (as conceptualized in the vast majority of catchment-scale conceptual
112 hydrological models) as the actual input signal already reaching the stream, while in reality it
113 is the remainder of past input signals that slowly travelled through the system (Hrachowitz et
114 al., 2016). The observable hydrological response therefore acts at different time scales than the
115 tracer response (Hrachowitz et al., 2016) as described by the celerity vs. velocity concept
116 (McDonnell and Beven, 2014). The observed patterns in our catchment therefore inspired us to
117 use a combined approach of hydrodynamic data analyses, stable water isotope investigations,
118 and data-driven hydrological modelling to determine catchment dynamics (response times and
119 groundwater age patterns) and unravel water flow paths at multiple spatial scales. This work
120 should further improve our knowledge on hydrological flow paths in developed, human-
121 impacted catchments.

122 2 Materials and methods

123 2.1 Study area

124 The research was carried out in the Schwingbach catchment (50°30'4.23"N, 8°33'2.82"E)
125 (Germany) (Fig. 1a). The Schwingbach and its main tributary the Vollnkirchener Bach are low-
126 mountainous creeks having an altitudinal difference of 50–100 m over 5 km distance (Perry and
127 Taylor, 2009) (Fig. 1c) with an altered physical structure of the stream system (channelled
128 stream reaches, pipes, drainage systems, fishponds). The Schwingbach catchment (9.6 km²)
129 ranges from 233–415 m a.s.l. with an average slope of 8.0%. The Vollnkirchener Bach tributary
130 is 4.7 km in length and drains a 3.7 km² subcatchment area (Fig. 1c), with elevations from 235–
131 351 m a.s.l. Almost 46% of the overall Schwingbach catchment is forested, which slightly
132 exceeds agricultural land use (35%) (Fig. 1c). Grassland (10%) is mainly distributed along
133 streams and smaller meadow orchards are located around the villages.

134 The Schwingbach main catchment is underlain by argillaceous shale in the northern parts,
135 serving as aquicludes. Graywacke zones with lydite in the central, as well as limestone, quartzite,
136 and sandstone regions in the headwater area provide aquifers with large storage capacities (Fig.
137 1f). Loess covers Paleozoic bedrock at north- and east bounded hillsides (Fig. 1f). Streambeds
138 consists of sand and debris covered by loam and some larger rocks (Lauer et al., 2013). Many
139 downstream sections of both creeks are framed by armor stones (Orlowski et al., 2014). The
140 dominant soil types in the overall study area are Stagnosols (41%) and mostly forested
141 Cambisols (38%). Stagnic Luvisols with thick loess layers, Regosol, Luvisols, and Anthrosols
142 are found under agricultural use and Gleysols under grassland along the creeks.

143 [Figure 1 near here]

144 The climate is classified as temperate with a mean annual temperature of 8.2°C. An annual
145 precipitation sum of 633 mm (for the hydrological year 1 November 2012 to 31 October 2013)
146 was measured at the catchment's climate station (site 13, Fig. 1b). The year 2012 to 2013 was
147 an average hydrometeorological year. For comparison, the climate station Giessen/Wettenberg
148 (25 km N of the catchment) operated by the German Meteorological Service (DWD, 2014)
149 records a mean annual temperature of 9.6 °C and a mean annual precipitation sum of 666±103
150 mm for the period 1980–2010. Discharge peaks from December to April (measured by the use
151 of RBC-flumes with maximum peak flow of 114 L s⁻¹, Eijkelkamp Agrisearch Equipment,
152 Giesbeek, NL) and low flows occur from July until November. Substantial snowmelt peaks

153 were observed during December 2012 and February 2013. Furthermore, May 2013 was an
154 exceptional wet month characterised by discharge of 2–3 mm d⁻¹. A detailed description of
155 runoff characteristics is given by Orłowski et al. (2014).

156 **2.2 Monitoring network and water isotope sampling**

157 The monitoring network consists of an automated climate station (site 13, Fig. 1 b–c) (Campbell
158 Scientific Inc., AQ5, UK; equipped with a CR1000 data logger), three tipping buckets, and 15
159 precipitation collectors, six stream water sampling points, and 22 piezometers (Fig. 1 b–c).
160 Precipitation data were corrected according to Xia (2006).

161 Two stream water sampling points (sites 13 and 18) in the Vollnkirchener Bach are installed
162 with trapezium shaped RBC-flumes for gauging discharge (Eijkelkamp Agrisearch Equipment,
163 Giesbeek, NL), and a V-weir is located at sampling point 64. RBC-flumes and V-weir are
164 equipped with Mini-Divers® (Eigenbrodt Inc. & Co. KG, Königsmoor, DE) for automatically
165 recording water levels. Discharge at the remaining stream sampling points was manually
166 measured applying the salt dilution method (WTW-cond340i, WTW, Weilheim, DE). The 22
167 piezometers (Fig. 1b) are made from perforated PVC tubes sealed with bentonite at the upper
168 part of the tube to prevent contamination by surface water. For monitoring shallow groundwater
169 levels, either combined water level/temperature loggers (Odyssey Data Flow System,
170 Christchurch, NZ) or Mini-Diver® water level loggers (Eigenbrodt Inc. & Co. KG,
171 Königsmoor, DE) are installed. Accuracy of Mini-Diver® is ±5 mm and for Odyssey data
172 logger ±1 mm. For calibration purposes, groundwater levels are additionally measured
173 manually via an electric contact gauge.

174 Stable water isotope samples of rainfall, stream-, and groundwater were taken from July 2011
175 to July 2013 on weekly intervals. In winter 2012–2013, snow core samples over the entire snow
176 depth of <0.15 m were collected in tightly sealed jars at same sites as open rainfall was sampled.
177 We sampled shortly after snow fall because sublimation, recrystallization, partial melting,
178 rainfall on snow, and redistribution by wind can alter the isotopic composition (Clark and Fritz,
179 1997b). Samples were melted overnight following Kendall and Caldwell (1998) and analysed
180 for their isotopic composition. Open rainfall was collected in self-constructed samplers as per
181 Windhorst et al. (2013). Grab samples of stream water were taken at six locations, three
182 sampling points at each stream (Fig. 1b–c). Since spatial isotopic variations of groundwater
183 among piezometers under meadow were small, samples were collected at three out of eight

184 sampling points under meadow (sites 1, 6, and 21), five under the arable field (sites 25–29), and
185 four next to the Vollnkirchener Bach (sites 24, 31, 32, and 35) (Fig. 1b). Additionally, a
186 drainage pipe (site 15) located ~226 m downstream of site 18 was sampled. According to IAEA
187 standard procedures, all samples were filled and stored in 2 mL brown glass vials, sealed with
188 a solid lid, and wrapped up with Parafilm®.

189 **2.3 Isotopic soil sampling**

190 **2.3.1 Spatial variability**

191 In order to analyse the effect of small-scale characteristics such as distance to stream, TWI, and
192 land use on soil isotopic signatures, we sampled a snapshot of 52 points evenly distributed over
193 a 200 m grid around the Vollnkirchener Bach (Fig. 1d). Soil samples were taken at four
194 consecutive rainless days (1 to 4 November 2011) at elevations of 235–294 m a.s.l.. Sampling
195 sites were selected via a stratified, GIS-based sampling plan (ArcGIS, Arc Map 10.2.1, Esri,
196 California, USA), including three classes of topographic wetness indices (TWIs: 4.4–6.5; 6.5–
197 7.7; 7.7–18.4), two different distances to stream (0–121 m, 121–250 m), and three land uses
198 (arable land, forest, and grassland), with each class containing the same number of sampling
199 points. Samples were collected at depths of 0.2 m and 0.5 m. Gravimetric water content was
200 measured according to DIN-ISO 11465 by drying soils for 24 h at 110 °C. Soil pH was analysed
201 following DIN-ISO 10390 on 1:1 soil-water-mixture with a handheld pH-meter (WTW
202 cond340i, WTW Inc., DE). Bulk density was determined according to DIN-ISO 11272, and soil
203 texture by finger testing.

204 **2.3.2 Seasonal isotope soil profiling and isotope analysis**

205 In order to trace the seasonal development of stable water isotopes from rainfall to groundwater,
206 seven soil profiles were taken in the dry summer season (28 August 2011), seven in the wet
207 winter period (28 March 2013), and two profiles in spring (24 April 2013) under different
208 vegetation cover (arable land and grassland) (Fig. 1d). Soil was sampled utilising a hand-auger
209 (Eijkelkamp Agrisearch Equipment BV, Giesbeek, DE) from the soil surface to 2 m depth.
210 Samples were collected in greater detail near the soil surface since this area is known to have
211 the greatest isotopic variability (Barnes and Allison, 1988).

212 Soil samples were stored in amber glass tubes, sealed with Parafilm®, and kept frozen until
213 water extraction. Soil water was extracted cryogenically with 180 min extraction duration, a

214 vacuum threshold of 0.3 Pa, and an extraction temperature of 90°C following Orłowski et al.
215 (2013). Isotopic signatures of $\delta^{18}\text{O}$ and $\delta^2\text{H}$ were analysed via off-axis integrated cavity output
216 spectroscopy (OA-ICOS) (DLT-100, Los Gatos Research Inc., Mountain View, USA). Within
217 each isotope analysis three calibrated stable water isotope standards of different water isotope
218 ratios were included (LGR working standard number 1, 3, and 5; Los Gatos Research Inc., CA,
219 US). After every fifth sample the LGR working standards are measured. For each sample, six
220 sequential 900 μL aliquot of a water sample are injected into the analyser. Then, the first three
221 measurements are discarded. The remaining are averaged and corrected for per mil scale
222 linearity following the IAEA laser spreadsheet template (Newman et al., 2009). Following this
223 IAEA standard procedure allows for drift and memory corrections. Isotopic ratios are reported
224 in per mil (‰) relative to Vienna Standard Mean Ocean Water (VSMOW) (Craig, 1961b).
225 Accuracy of analyses was 0.6‰ for $\delta^2\text{H}$ and 0.2‰ for $\delta^{18}\text{O}$ (LGR, 2013). Leaf water extracts
226 typically contain a high fraction of organic contaminations, which might lead to spectral
227 interferences when using isotope ratio infrared absorption spectroscopy, causing erroneous
228 isotope values (Schultz et al., 2011). However, for soil water extracts there exists no need to
229 check or correct such data (Schultz et al., 2011; Zhao et al., 2011).

230 **2.4 Mean transit time estimation**

231 To understand the connection between the different water cycle components in the
232 Schwingbach catchment, mean transit times (MTT) for both streams as well as from
233 precipitation to groundwater were calculated using FlowPC (Maloszewski and Zuber, 2002).
234 See Appendix I for details about the applied method.

235 **2.5 Model-based groundwater age dynamics**

236 To estimate the age dynamics of the groundwater body in the Vollnkirchener Bach
237 subcatchment, a hydrological model was established on the basis of the conceptual model
238 presented by Orłowski et al. (2014) and the isotopic measurements presented here. Appendix
239 II outlines the modelling concept, model set up, and its parameterization.

240 **2.6 Statistical analyses**

241 For statistical analyses, we used IBM SPSS Statistics (Version 22, SPSS Inc., Chicago, IL, US)
242 and R (version Rx64 3.2.2). The R package igraph was utilized for plotting (Csardi and Nepusz,

243 2006). Studying temporal and spatial variations in meteoric and groundwater, isotope data were
244 tested for normal distribution. Subsequently, t-tests or Multivariate Analyses of Variances
245 (MANOVAs) were applied and Tukey-HSD tests were run to determine which groups were
246 significantly different ($p \leq 0.05$). Event mean values of isotopes in precipitation, stream, and
247 groundwater were calculated when no spatial variation was observed. Regression analyses were
248 run to determine the effect of small-scale characteristics such as distance to stream, TWI, and
249 land use on soil isotopic signatures.

250 We used a topology inference network map (Kolaczyk, 2014) in combination with a principal
251 component analysis to show $\delta^{18}\text{O}$ isotope relationships between surface and groundwater
252 sampling points. To explore the sensitivity of missing data, we used both the complete isotope
253 time series and randomly selected 80% of the whole data sets. Overall, the cluster relationships
254 of the surface and groundwater sampling points are largely similar for both whole and subsets
255 of isotope data sets, despite some differences of the exact cluster centroid locations. We
256 therefore decided to use randomly selected 80% of the isotope time series to illustrate our
257 results. In the network map, each node of the network represents an isotope sampling point.
258 The locations of the nodes are based on the first two components (PC1 and PC2). The
259 correlations between isotope time series are represented by the edges connecting nodes. The
260 thickness of edges characterizes the strength of the correlations. The p-values of correlations
261 are approximated by using the F-distributions and mid-ranks are used for the ties (Hollander et
262 al., 2013). Only statistically significant connections ($p < 0.05$) are shown.

263 To compare different water sources on the catchment-scale, a local meteoric water (LMWL)
264 line was developed and evaporation water lines (EWLs) were used. They represent the linear
265 relationship between $\delta^2\text{H}$ and $\delta^{18}\text{O}$ of meteoric waters (Cooper, 1998) in contrast to the global
266 meteoric water line (GMWL), which describes the world-wide average stable isotopic
267 composition in precipitation (Craig, 1961a). Identifying the origin of water vapour sources and
268 moisture recycling (Gat et al., 2001; Lai and Ehleringer, 2011), the deuterium-excess (d-
269 excess), defined by Dansgaard (1964) as $d = \delta^2\text{H} - 8 \times \delta^{18}\text{O}$ was used.

270 For comparisons, precipitation isotope data from the closest GNIP (Global Network of Isotopes
271 in Precipitation) station Koblenz (DE; 74 km SW of the study area, 97 m a.s.l.) was used (IAEA,
272 2014; Stumpp et al., 2014). For monthly comparisons with Schwingbach d-excess values, we
273 used a data set from the GNIP station Koblenz that includes 24 values starting from July 2011
274 to July 2013.

275 3 Results

276 3.1 Variations of precipitation isotopes and d-excess

277 The $\delta^2\text{H}$ values of all precipitation isotope samples ranged from -167.6 to -8.3‰ (Table 1). To
278 examine the spatial isotopic variations, rainfall was collected at 15 open field site locations
279 throughout the Schwingbach main catchment (Fig. 1b–c) for a 7-month period, but no spatial
280 variation could be observed. Thus, rainfall was collected at the catchment outlet (site 13) from
281 23 October 2014 onward. We could neither identify an amount effect nor an altitude effect in
282 our precipitation isotope data. The greatest altitudinal difference between sampling points was
283 also only 101 m. Nevertheless, a slight temperature effect ($R^2=0.5$ for $\delta^2\text{H}$ and $R^2=0.6$ for $\delta^{18}\text{O}$,
284 respectively) was observed showing enriched isotopic signatures at higher temperatures.

285 [Table 1 near here]

286 Strong temporal variations in precipitation isotopic signatures, as well as pronounced seasonal
287 isotopic effects were measured with greatest isotopic differences occurring between summer
288 and winter. Samples taken in the fall and spring were isotopically similar, however, differed
289 from winter isotopic signature, which were somewhat lighter (Fig. 2). Furthermore, in the
290 winter of 2012–13 snow was sampled, which decreased the mean winter isotopic values for this
291 period in comparison to the previous winter period (2011–12) where no snow sampling could
292 be conducted. The mean $\delta^2\text{H}$ isotope values of snow samples were approximately 84‰ lighter
293 than mean precipitation isotopic signatures (Fig. 3). Furthermore, no statistically significant
294 ($p>0.05$) inter-annual variation was detected between the summer periods of 2011 and 2012
295 (Fig. 2).

296 [Figure 2 near here]

297 Examining the influence of moisture recycling on the isotopic compositions of precipitation,
298 the d-excess was calculated for each individual rain event at the Schwingbach catchment. D-
299 excess values ranged from -7.8‰ to $+19.4\text{‰}$ and averaged $+7.1\text{‰}$ (Fig. 2). In general, 37% of
300 all events were sampled in summer periods (21 June to 21/22 September). These summer events
301 showed lower d-excess values in comparison to the 19% winter precipitation events (21/22
302 December to 19/20 March) (Fig. 2). D-excess greater than $+10\text{‰}$ was determined for 22% of
303 all events. Lowest values corresponded to summer precipitation events where evaporation of
304 the raindrops below the cloud base may occur. Most of the higher values ($>+10\text{‰}$) appeared in

305 cold seasons (fall/winter) and winter snow samples of the Schwingbach catchment with much
306 depleted δ -values showed highest d-excess (Fig. 2).

307 In comparison with the GNIP station Koblenz (2011–2013), the mean annual d-excess at the
308 Schwingbach catchment was on average 3.9‰ higher, showing a greater impact of oceanic
309 moisture sources than the further south-west located station Koblenz. The long-term mean d-
310 excess was 4.4‰ for the Koblenz station (1978–2009) (Stumpp et al., 2014). Highest d-
311 excesses at the GNIP station matched highest values in the Schwingbach catchment, both
312 occurring in the cold seasons (October to December 2011 and November to December 2012).

313 The linear relationship of $\delta^2\text{H}$ and $\delta^{18}\text{O}$ content in local precipitation, results in a local meteoric
314 water line (LMWL) (Fig. 3). The slope of the Schwingbach LMWL is well in agreement with
315 the one from the GNIP station Koblenz ($\delta^2\text{H}=7.66\times\delta^{18}\text{O}+2.0\text{‰}$; $R^2=0.97$; 1978–2009 (Stumpp
316 et al., 2014)), but is slightly lower in comparison to the GMWL, showing stronger local
317 evaporation conditions. Since evaporation causes a differential increase in $\delta^2\text{H}$ and $\delta^{18}\text{O}$ values
318 of the remaining water, the slope for the linear relationship between $\delta^2\text{H}$ and $\delta^{18}\text{O}$ is lower in
319 comparison to the GMWL (Rozanski et al., 2001; Wu et al., 2012).

320 [Figure 3 near here]

321 **3.2 Isotopes of soil water**

322 **3.2.1 Spatial variability**

323 Determining the impact of landscape characteristics on soil water isotopic signatures, we found
324 no statistically significant connection between the parameters distance to stream, TWI, soil
325 water content, soil texture, pH, and bulk density with the soil isotopic signatures in both soil
326 depths, except for land use.

327 [Table 2 near here]

328 The mean δ -values in the top 0.2 m of the soil profile are higher than in the subsoil, reflecting
329 a stronger impact of precipitation in the topsoil (Table 2, Fig. 4). While the δ -values for subsoil
330 and precipitation differed significantly ($p\leq 0.05$), they did not for topsoil (Fig. 4). Subsoil
331 isotopic values were statistically equal to stream water and groundwater (Fig. 4).

332 [Figure 4 near here]

333 Generally, all soil water isotopic values fell on the LMWL, indicating no evaporative
334 enrichment (Fig. 5). Comparing soil isotopic signatures between different land covers showed
335 generally higher and statistically significantly different δ -values ($p \leq 0.05$) at 0.2 m soil depth
336 under arable land as compared to forests and grasslands. For the lower 0.5 m of the soil column,
337 isotopic signatures under all land uses showed statistically similar values. Comparing soil water
338 $\delta^2\text{H}$ values between top and subsoil under different land use units showed significant
339 differences ($p \leq 0.05$) under arable and grassland but not under forested sites (Fig. 5).

340 [Figure 5 near here]

341 **3.2.2 Seasonal isotope soil profiling**

342 Isotope compositions of soil water varied seasonally: More depleted soil water was found in
343 the winter and spring (Fig. 6); contrary, soil water was enriched in summer due to evaporation
344 during warmer and drier periods (Darling, 2004). For summer soil profiles in the Vollnkirchener
345 subcatchment, no evidence for evaporation was obvious below 0.4 m soil depth. However,
346 snowmelt isotopic signatures could be traced down to a soil depth of 0.9 m during spring rather
347 than winter, pointing to a depth-translocation of meltwater in the soil, more remarkable for the
348 deeper profile under arable land (Fig. 6, upper left panel). Furthermore, shallow soil water (<0.4
349 m) showed larger standard deviations with values closer to mean seasonal precipitation inputs
350 (Fig. 6, upper panels). Winter profiles exhibited somewhat greater standard deviations in
351 comparison to summer isotopic soil profiles. The observed seasonal amplitude became less
352 pronounced with depth as soil water isotope signals approached groundwater average in >0.9 m
353 depth. Generally, deeper soil water isotope values were relatively constant through time and
354 space.

355 [Figure 6 near here]

356 **3.3 Isotopes of stream water**

357 No statistically significant differences were found between the Schwingbach and
358 Vollnkirchener Bach stream water (Fig. 7). All stream water isotope samples fell on the LMWL
359 except for few evaporatively enriched samples (Fig. 3). $\delta^{18}\text{O}$ values varied for the
360 Vollnkirchener Bach by $-8.4 \pm 0.4\text{‰}$ and for the Schwingbach by $-8.4 \pm 0.6\text{‰}$ (Table 1). Stream
361 water isotopic signatures were by approximately -15‰ in $\delta^2\text{H}$ more depleted than precipitation
362 signatures and similar to groundwater (Table 1).

364 A damped seasonality of the isotope concentration in stream water versus precipitation was
365 occurring between summer and winter (Fig. 7). Most outlying depleted stream water isotopic
366 signatures (e.g. in March 2012 and 2013) can be explained by snowmelt (Fig. 7). However, the
367 outlier at the Schwingbach stream water sampling site 64 (-66.7‰ for $\delta^2\text{H}$) is by 8.5‰ more
368 depleted than the two-year average of Schwingbach stream water (Table 1). Rainfall falling on
369 24 September 2012 was -31.9‰ for $\delta^2\text{H}$. This period in September was generally characterized
370 by low flow and little rainfall. Thus, little contribution of new water was observed and stream
371 water isotopic signatures were groundwater-dominated. For site 13, the outlier in May 2012
372 (-44.2‰ for $\delta^2\text{H}$) was by 13.8‰ more enriched than the average stream water isotopic
373 composition of the Vollnkirchener Bach over the two-year observation period (Table 1). A
374 runoff peak at site 13 of 0.15 mm d^{-1} and a 2.9 mm rainfall event were recorded on 23 May
375 2012. Thus, this outlier could be explained by precipitation contributing to stream flow causing
376 more enriched isotopic values in stream water, which approached average precipitation δ -values
377 (-43.9 ± 23.4).

378 MTT calculations for the Schwingbach and the Vollnkirchener Bach did not provide a good fit
379 in terms of the quality criteria sigma and model efficiency (Timbe et al., 2014) ($\text{ME}_{\text{Schwingbach}}$
380 -0.1 – 0.0 , $\text{ME}_{\text{Vollnkirchener Bach}}$ 0.0 – 0.4 ; sigma for all sampling points 0.1). Bias correction of the
381 input data did not improve the model outputs (sigma= 0.1).

382 **3.4 Isotopes of groundwater**

383 For the piezometers under meadow, almost constant isotopic values (Fig. 8, Table 1) were
384 observed ($\delta^2\text{H}$: $-57.6 \pm 1.6\text{‰}$). Most depleted groundwater isotopic values ($< -80\text{‰}$ for $\delta^2\text{H}$)
385 were measured for piezometer 32 during snowmelt events in March and April 2013 as well as
386 for piezometer 27 from December 2012 to February 2013. Piezometer 32 is highly responsive
387 to rainfall-runoff events and groundwater head elevations showed significant correlations with
388 mean daily discharge at this site (Orlowski et al., 2014).

389 Groundwater under meadow differed from mean precipitation values by about -14‰ for $\delta^2\text{H}$
390 showing no evidence of a rapid transfer of rainfall isotopic signatures to the groundwater (Fig.
391 8). For the MTT estimations of the thirteen piezometers, the calculated output data did not fit
392 the observed values showing very low MEs (ME: -0.62 – -0.09 for $\delta^{18}\text{O}$ and -0.49 – 0.16 for
393 $\delta^2\text{H}$; sigma: 0.08 – 0.15 for $\delta^{18}\text{O}$ and 0.62 – 1.11 for $\delta^2\text{H}$).

394

[Figure 8 near here]

395 Due to different water flow paths of groundwater along the studied stream, we expected to find
396 distinguished groundwater isotopic signatures. In fact, we could identify spatial statistical
397 differences between grassland and arable land groundwater isotopic signatures (Fig. 9).
398 Groundwater isotopic signatures under arable land (sites: 25–29, Fig. 1b) showed more
399 enriched values (Fig. 8) and showed significant correlations ($p < 0.05$) among each other (Fig.
400 9). Arable land groundwater plotted furthest away from surface water sampling points in our
401 network map showing no significant correlations to either the Schwingbach or the
402 Vollnkirchener Bach. $\delta^{18}\text{O}$ time series of piezometers along the stream and under the meadow
403 showed closest relations to surface water sampling points (Fig. 9). We further found high
404 correlations ($R^2 > 0.6$) of $\delta^{18}\text{O}$ time series of piezometers located under the meadow among each
405 other. Additionally, $\delta^{18}\text{O}$ values of piezometer 3 correlated significantly ($p < 0.05$) with surface
406 water sampling points 18 and 94 ($R^2 = 0.6$ and 0.8 , respectively) and piezometer 32 with
407 sampling points 13 and 64 ($R^2 = 0.8$ and 0.6 , respectively).

408

[Figure 9 near here]

409 We further observed close relations ($p < 0.05$) among $\delta^{18}\text{O}$ values of Vollnkirchener Bach
410 sampling sites 13, 18, and 94 as well as of Schwingbach sites 11, 19, and 64 along with
411 significant correlations between each other.

412 **3.5 Groundwater age dynamics**

413 Since MTT calculations did not provide a good fit between the observed and calculated output
414 data, we modelled the groundwater age in the Vollnkirchener Bach subcatchment using CMF
415 (Appendix II), applying observed hydrometric as well as stable water isotope data (Fig. 10).

416

[Figure 10 near here]

417 The maximum age of water is highly variable throughout the subcatchment, which results in a
418 heterogeneous spatial age distribution. The groundwater in most of the outer cells is young (0–
419 10 years), whereas the inner cells, which incorporate the Vollnkirchener Bach, contain older
420 water (> 30 years). The oldest water (≥ 55 years) can be found in the Northern part of the
421 catchment (Fig. 10, detail view), where the Vollnkirchener Bach drains into the Schwingbach.
422 The main outlets of the subcatchment (dark red coloured cell and green cell) even reach an age
423 of 100 and 55 years, respectively. This can be explained by the fact that it is the lowest cell

424 within the subcatchment and that water accumulates here. The overall flow path to this cell is
425 the longest and as a consequence the groundwater age in this cell is the highest.

426 In general, 2% of cells contain groundwater that is older than 50 years, <1% reveal ages >70
427 years, 13% contain water with an age of less than one year, and 52% with an age <15 years.
428 Thus, most of the cells contain young to moderately old water (<15 years), while few cells
429 comprise old water (>50 years). The average groundwater age in the Vollnkirchener Bach
430 subcatchment is 16 years. Correlating the groundwater age against the distance to the stream,
431 we found a linear correlation ($R^2=0.3$) with a distinct trend. The water tends to be younger with
432 greater distance to the stream.

433 The amount of flowing water depicted by the length of the arrows is generally higher near the
434 stream, whereas in most of the outer cells the amount is very low (Fig. 10). The modelled main
435 flow direction is towards the Vollnkirchener Bach but many arrows show flow direction across
436 the stream indicating bidirectional water exchange between the stream and the groundwater
437 body.

438 **4 Discussion**

439 **4.1 Variations of precipitation isotopes and d-excess**

440 We found no spatial variation in precipitation isotopes throughout the Schwingbach catchment.
441 Mook et al. (1974) also observed for north-western Europe that precipitation collected over
442 periods of 8 and 24 h from three different locations within 6 km² at the same elevation were
443 consistent within 0.3‰ for $\delta^{18}\text{O}$. Further, we detected no amount or altitude effect on isotopes
444 in precipitation. Amount effects generally occur most likely in the tropics or for intense
445 convective rain events and are not a key factor for explaining isotope distributions in German
446 precipitation (Stumpp et al., 2014).

447 The observed linear relationship ($\delta^{18}\text{O}=0.44T-12.05\text{‰}$) between air temperature and
448 precipitation $\delta^{18}\text{O}$ values compares reasonably well with a correlation reported by Yurtsever
449 (1975) based on north Atlantic and European stations from the GNIP network
450 $\delta^{18}\text{O}=(0.521\pm 0.014)T-(14.96\pm 0.21)\text{‰}$. The same is true for a correlation found by Rozanski et
451 al. (1982) for the GNIP station Stuttgart, 196 km South of the Schwingbach. Stumpp et al.
452 (2014) analysed long-term precipitation data from meteorological stations across Germany and
453 found that 23 out of 24 tested stations showed a positive long-term temperature trend over time.
454 The observed correspondence between the degree of isotope depletion and the temperature

455 reflects the influence of the temperature effect in the Schwingbach catchment, which mainly
456 appears in continental, middle–high latitudes (Jouzel et al., 1997). Furthermore, the correlation
457 between $\delta^2\text{H}$ in monthly precipitations and local surface air temperature becomes increasingly
458 stronger towards the centre of the continent (Rozanski et al., 1982). Thus, the observed seasonal
459 differences in precipitation δ -values in the Schwingbach catchment could mainly be attributed
460 to seasonal differences in air temperature and the presence of snow in the winter of 2012–13
461 (Fig. 2).

462 Precipitation events originating from oceanic moisture show d-excess values close to +10‰
463 (Craig, 1961a; Dansgaard, 1964; Wu et al., 2012) and one of the main sources for precipitation
464 in Germany is moisture from the Atlantic Ocean (Stumpp et al., 2014). Lowest values
465 corresponded to summer precipitation events where evaporation of the falling raindrops below
466 the cloud base occurs. Same observations were made by Rozanski et al. (1982) for European
467 GNIP stations. Winter snow samples of the Schwingbach catchment with very depleted δ -
468 values showed highest d-excess values ($>+10\%$), well in agreement with results of Rozanski et
469 al. (1982) for European GNIP stations. The observed differences in d-excess values between
470 the Schwingbach catchment and the GNIP station Koblenz can be attributed to differences in
471 elevation range and the different regional climatic settings at both sites (Koblenz is located in
472 the relatively warmer Rhine river valley).

473 **4.2 Isotopes of soil water**

474 **4.2.1 Spatial variability**

475 We found no statistically significant connection between the parameters distance to stream,
476 TWI, soil water content, soil texture, pH, and bulk density with the soil isotopic signatures in
477 both soil depths. This was potentially attributed to the small variation in soil textures (mainly
478 clayey silts and loamy sandy silts), bulk densities, and pH values for both soil depths (Table 2).
479 Garvelmann et al. (2012) obtained high resolution $\delta^2\text{H}$ vertical depth profiles of pore water at
480 various points along two fall lines of a pasture hillslope in the Black Forest (Germany) by
481 applying the $\text{H}_2\text{O}(\text{liquid})\text{--}\text{H}_2\text{O}(\text{vapor})$ equilibration laser spectroscopy method. The authors
482 showed that groundwater was flowing through the soil in the riparian zone (downslope profiles)
483 and dominated streamflow during baseflow conditions. Their comparison indicated that the
484 percentage of pore water soil samples with a very similar stream water $\delta^2\text{H}$ signature is
485 increasing towards the stream channel (Garvelmann et al., 2012). In contrast, we found no such

486 relationship between the distance to stream or TWI and soil isotopic values in the
487 Vollnkirchener Bach subcatchment over various elevations (235–294 m a.s.l.) and locations.
488 We attributed this to the gentle hillslopes and the low subsurface flow contribution in large
489 parts of the catchment.

490 In our study, the δ -values of top soil and precipitation did not differ statistically (Fig. 4), but for
491 precipitation and subsoil they did. The latter indicates either the influence of evaporation in the
492 topsoil or the mixing with groundwater in the subsoil. However, a mixing and homogenization
493 of new and old soil water with depth could not clearly be seen in 0.5 m soil depth, which would
494 have resulted in a lower standard deviation (Song et al., 2011), but standard deviations of
495 isotopic signatures in top and subsoil were similar (Table 2). Subsoil isotopic values were
496 statistically equal to stream water and groundwater (Fig. 4) implying that capillary rise of
497 groundwater occurred. Overall, the rainfall isotopic signal was not directly transferred through
498 the soil to the groundwater; even so groundwater head level rose promptly after rainfall events.
499 This behaviour reflects the differences of celerity and velocity in the catchment's rainfall-runoff
500 response (McDonnell and Beven, 2014).

501 Soil water $\delta^2\text{H}$ between top and subsoil showed significant differences ($p \leq 0.05$) under arable
502 and grassland but not under forested sites (Fig. 5). This could be explained through the
503 occurrence of vertical preferential flow paths and interconnected macropore flow (Buttle and
504 McDonald, 2002) characteristic for forested soils. Alaoui et al. (2011) showed that macropore
505 flow with high interaction with the surrounding soil matrix occurred in forest soils, while
506 macropore flow with low to mixed interaction with the surrounding soil matrix dominates in
507 grassland soils. Seasonal tilling prevents the establishment of preferential flow paths under
508 agricultural sites and is regularly done in the Schwingbach catchment, whereas the structure of
509 forest soils, may remain uninterrupted throughout the entire soil profile for years (in particular
510 the macropores and biopores) (Alaoui et al., 2011). This is reflected in the bulk density of the
511 soils in the Schwingbach catchment that increases from forests (1.10 g cm^{-3}) over grassland
512 (1.25 g cm^{-3}) to arable land (1.41 g cm^{-3}) in the top soil. We infer that reduced hydrological
513 connection between top and subsoil under arable and grassland led to different isotopic
514 signatures (Fig. 5).

515 Although, vegetation cover has often shown an impact on soil water isotopes (Gat, 1996), only
516 few data are available for Central Europe (Darling, 2004). Burger and Seiler (1992) found that
517 soil water isotopic enrichment under spruce forest in Upper Bavaria was double that beneath

518 neighbouring arable land but soil isotope values were not comparable to groundwater (Burger
519 and Seiler, 1992). Gehrels et al. (1998) also detected (though only slightly) heavier isotopic
520 signatures under forested sites in the Netherlands in comparison to non-forested sites (grassland
521 and heathland). Contrasting, in southern Germany Brodersen et al. (2000) observed only a
522 negligible effect of throughfall isotopic signatures (of spruce and beech) on soil water isotopes,
523 since soil water in the upper layers followed the seasonal trend in the precipitation input and
524 had a very constant signature in greater depth. In a study by Sprenger et al. (2016b) the
525 differences between the investigated soil profiles across the Aart catchment (LU) were mostly
526 driven by soil types which was also seen in the pore water stable isotope dynamics reported for
527 soils in the Scottish Highlands (Geris et al., 2015). However, for the Schwingbach catchment
528 we conclude that the observed land use effect in the upper soil column is mainly attributed to
529 different preservation and transmission of the precipitation input signal. It is most likely not
530 attributable to distinguished throughfall isotopic signatures, impact of evaporation or
531 interception losses, since top soil water isotopic signals followed the precipitation input signal
532 under all land use units.

533 **4.2.2 Seasonal isotope soil profiling**

534 Soil water was enriched in summer due to evaporation during warmer and drier periods. The
535 depth to which soil water isotopes are significantly affected by evaporation is rarely more than
536 1–2 m below ground, and often less under temperate climates (Darling, 2004). In contrast,
537 winter profiles exhibited somewhat greater standard deviations in comparison to summer
538 isotopic soil profiles, indicative for wetter soils (Fig. 6, lower panels) and shorter residence
539 times (Thomas et al., 2013). Isotope profiles taken during or after snow melt in a study by
540 Sprenger et al. (2016b) did not show an isotopic depletion at a certain depth as observed for
541 example by Stumpp and Hendry (2012) and Peralta-Tapia et al. (2015). Generally, deeper soil
542 water isotope values in our study were relatively constant through time and space. Similar
543 findings were made by Foerstel et al. (1991) on a sandy soil in western Germany, McConville
544 et al. (2001) under predominately agriculturally used Gley and till soils in Northern Ireland,
545 Thomas et al. (2013) in a forested catchment in central Pennsylvania, USA, and Bertrand et al.
546 (2014) on the Pfyf alluvial forest (CH). Furthermore, Tang and Feng (2001) showed for a sandy
547 loam in New Hampshire (USA) that the influence of summer precipitation decreased with
548 increasing depth, and soils at 0.5 m only received water from large storms. Pore water $\delta^2\text{H}$
549 profiles taken at the catchment of the groundwater aquifer Freiburger Bucht (DE) in a study by

550 Sprenger et al. (2016a) showed how the isotopic signal of rain water over time is preserved in
551 the unsaturated soil profile. However, the input signal was dampened due to mixing processes.
552 In our summer soil profiles under arable land, precipitation input signals decreased with depth
553 (Fig. 6, upper left panel). Dampening of precipitation's isotopic fluctuations with increasing
554 soil depth was in line with other studies (e.g. Muñoz-Villers and McDonnell, 2012; Timbe et
555 al., 2014; Wang et al., 2010). Generally, the replacement of old soil water with new infiltrating
556 water is dependent on the frequency and intensity of precipitation and the soil texture, structure,
557 wetness, and water potential of the soil (Li et al., 2007; Tang and Feng, 2001). As a result, the
558 amount of percolating water decreases with depth and consequently, deeper soil layers have
559 less chance to obtain new water (Tang and Feng, 2001). In the growing season, the percolation
560 depth is additionally limited by plants' transpiration (Tang and Feng, 2001). For the
561 Schwingbach catchment we conclude that the percolation of new soil water is low as no
562 remarkable seasonality in soil isotopic signatures was obvious at >0.9 m and constant values
563 were observed through space and time. Although replications over several years are missing,
564 this result indicates a transit time through the rooting zone (1m) of approximately one year.

565 **4.3 Linkages between water cycle components**

566 Stream water isotopic time series of the Vollnkirchener Bach and Schwingbach showed little
567 deflections through time. Due to the observed isotopic similarities of stream and groundwater,
568 we conclude that groundwater predominantly feeds baseflow (discharge $<10 \text{ L}\cdot\text{s}^{-1}$). Even
569 during peak flow occurring in January 2012, December to April or May 2013, rainfall input did
570 not play a major role for stream water isotopic composition although fast rainfall-runoff
571 behaviours were observed by Orłowski et al. (2014). The damped groundwater isotopic
572 signatures seemed to be a mixture of former lighter precipitation events and snowmelt, since
573 meltwater is known to be depleted in stable isotopes as compared to precipitation or
574 groundwater (Rohde, 1998) (Figure 3). However, differences in the snow sampling method
575 (new snow, snow pit layers, meltwater) can affect the isotopic composition (Penna et al., 2014;
576 Taylor et al., 2001). As groundwater at the observed piezometers in the Vollnkirchener
577 subcatchment is shallow (Orłowski et al., 2014), the snowmelt signal is able to move rapidly
578 through the soil. Pulses of snowmelt water causing a depletion in spring and early summer was
579 also observed by other studies (Darling, 2004; Kortelainen and Karhu, 2004). We therefore
580 conclude that groundwater is mainly recharged throughout the winter. During spring runoff
581 when soils are saturated, temperatures are low, and vegetation is inactive, recharge rates are

582 generally highest. In contrast, recharge is very low during summer when most precipitation is
583 transpired back to the atmosphere (Clark and Fritz, 1997a). Similarly, O'Driscoll et al. (2005)
584 showed that summer precipitation does not significantly contribute to recharge in the Spring
585 Creek watershed (Pennsylvania, USA) since $\delta^{18}\text{O}$ values in summer precipitation were enriched
586 compared to mean annual groundwater composition.

587 Further, Orlowski et al. (2014) showed that influent and effluent conditions (bidirectional water
588 exchange) occurred simultaneously at different stream sections of the Vollnkirchener Bach
589 affecting stream and groundwater isotopic compositions, equally. Our network map supported
590 this assumption (Fig. 9) as surface water sampling points plotted close to groundwater sampling
591 points (especially to the sampling points under the meadow and along the stream). This was
592 also underlined by our groundwater model showing flow directions across the Vollnkirchener
593 Bach. Nevertheless, both stream and groundwater differed significantly from rainfall isotopic
594 signatures (Table 1). Thus, our catchment showed double water paradox behaviour as per
595 Kirchner (2003) with fast release of very old water but little variation in tracer concentration.

596 **4.4 Water age dynamics**

597 Our MTT calculations did not provide a good fit between the observed and calculated data. Just
598 by comparing mean precipitation, stream, and groundwater isotopic signatures (Table 1), one
599 could expect that simple mixing calculations would not work to derive MTTs, i.e. showing
600 predominant groundwater contribution. Same observations were made by Jin et al. (2010)
601 indicating good hydraulic connectivity between surface water and shallow groundwater. Just as
602 in the here presented results, Klaus et al. (2015) had difficulties to apply traditional methods of
603 isotope hydrology (MTT estimation, hydrograph separation) to their dataset due to the lack of
604 temporal isotopic variation in stream water of a forested low-mountainous catchment in South
605 Carolina (USA). Furthermore, stable water isotopes can only be utilised for estimations of
606 younger water (<5 years) (Stewart et al., 2010) as they are blind to older contributions (Duvert
607 et al., 2016). In our catchment, transit times are orders of magnitudes longer than the timescale
608 of hydrologic response (prompt discharge of old water) (McDonnell et al., 2010) and the range
609 used for stable water isotopes.

610 Accurately capturing the transit time of the old water fraction is essential (Duvert et al., 2016)
611 and could previously only be determined via other tracers such as tritium (e.g. Michel (1992)).
612 Current studies on mixing assumptions either consider spatial or time-varying MTTs.

613 Heidbüchel et al. (2012) proposed the concept of the master transit time distribution that
614 accounts for the temporal variability of MTT. The time-varying transit time concept of Botter
615 et al. (2011) and van der Velde et al. (2012), was recently reformulated by Harman (2015) so
616 that the storage selection function became a function of the watershed storage and actual time.
617 Instead of quantifying time-variant travel times, our model facilitates the estimation of spatially
618 distributed groundwater ages, which opens up new opportunities to compare groundwater ages
619 from over a range of scales within catchments. It further gives a deeper understanding of the
620 groundwater-surface water connection across the landscape than a classical MTT calculation
621 could provide. Our work complements recent advances in spatially distributed modelling of age
622 distributions through transient groundwater flows (e.g. Gomez and Wilson, 2013; Woolfenden
623 and Ginn, 2009). The results of our model reveal a spatially highly heterogeneous age
624 distribution of groundwater throughout the Vollnkirchener Bach subcatchment (ages of 2 days–
625 100 years) with oldest water near the stream. Thus, our model provides the opportunity to make
626 use of stable water isotope information along with climate, land use, and soil type data, in
627 combination with a digital elevation map to estimate residence times >5 years. If stable water
628 isotope information is used alone, it is known to cause a truncation of stream residence time
629 distributions (Stewart et al., 2010). Further, our groundwater model suggests that the main
630 groundwater flow direction is towards and across the stream and the quantity of flowing water
631 is highest near the stream (Fig. 10). This further supports the assumption that stream water is
632 mainly fed by older groundwater. Moreover, the simulation underlines the conclusion that the
633 groundwater body and stream water are isotopically disconnected from the precipitation cycle,
634 since only 13% of cells contained water with an age <1 year.

635 However, our semi-conceptual model approach has also some limitations. During model setup
636 a series of assumptions and simplifications were made to develop a realistic hydrologic model
637 without a severe loss in performance. Due to the assumption of a constant groundwater recharge
638 over the course of a year, no seasonality was simulated. Moreover, no spatial differences in soil
639 properties of the groundwater layer were considered. Further, several parameters such as the
640 depth of the groundwater body are only rough estimations, while others like evapotranspiration
641 are based on simulations. Moreover, the groundwater body is highly simplified since e.g.
642 properties of the simulated aquifer are assumed to be constant over the subcatchment.
643 Nevertheless, as shown by the diverse ages of water in the stream cells and the assumption of
644 spatially gaining conditions, the model confirms that the stream contains water with different
645 transit times and supports the assumption that surface and groundwater are isotopically

646 disconnected from precipitation. Therefore, the stream water does not have a discrete age, but
647 a distribution of ages due to variable flow paths (Stewart et al., 2010). In future models a more
648 diverse groundwater body based on small-scale measurements of aquifer parameters should be
649 implemented. Especially data of saturated hydraulic conductivity with high spatial resolution,
650 as well as the implementation of a temporal dynamic groundwater recharge could lead to an
651 enhanced model performance.

652 **5 Conclusions**

653 Conducting a stable water isotope study in the Schwingbach catchment helped to identify
654 relationships between precipitation, stream, soil, and groundwater in a developed (managed)
655 catchment. The close isotopic link between groundwater and the streams revealed that
656 groundwater controls streamflow. Moreover, it could be shown that groundwater was
657 predominately recharged during winter but was decoupled from the annual precipitation cycle.
658 Even so streamflow and groundwater head levels promptly responded to precipitation inputs,
659 there was no obvious change in their isotopic composition due to rain events.

660 Nevertheless, the lack of temporal variation in stable isotope time series of stream and
661 groundwater limited the application of classical methods of isotope hydrology, i.e. transfer
662 function based MTT estimations. By splitting the flow path into different compartments (upper
663 and lower vadose zone, groundwater, stream), we were able to determine, where the water age
664 passes the limit of using stable isotopes for age calculations. This limit is in the lower vadose
665 zone approximately 1–2 m below ground. To estimate the total transit time to the stream, we
666 set up a hydrological model calculating spatially distributed groundwater ages and flow
667 directions in the Vollnkirchener Bach subcatchment. Our model results supported the finding
668 that the water in the catchment is >5 years (on average 16 years) and that stream water is mainly
669 fed by groundwater. Our modelling approach was valuable to overcome the limitations of MTT
670 calculations with traditional methods and/or models. Further, our dual isotope study in
671 combination with the hydrological model approach enabled the determination of connection
672 and disconnection between different water cycle components.

673 **Acknowledgements**

674 The first author acknowledges financial support by the Friedrich-Ebert-Stiftung (Bonn, DE).
675 Furthermore, this work was supported by the Deutsche Forschungsgemeinschaft under Grant
676 BR2238/10-1. Thanks also to the student assistants, BSc. and MSc. students for their help
677 during field sampling campaigns and hydrological modelling. In this regard we like to

678 acknowledge especially Julia Mechsner, Julia Klöver, and Judith Henkel. We thank Dr.
679 Christine Stumpp from the Helmholtz Zentrum München for providing us the isotope data from
680 GNIP station Koblenz.
681

682 **References**

- 683 Alaoui, A., Caduff, U., Gerke, H. H. and Weingartner, R.: Preferential Flow Effects on
684 Infiltration and Runoff in Grassland and Forest Soils, *Vadose Zone J.*, 10(1), 367,
685 doi:10.2136/vzj2010.0076, 2011.
- 686 Allan, J. D.: Landscapes and Riverscapes: The Influence of Land Use on Stream Ecosystems,
687 *Annu. Rev. Ecol. Evol. Syst.*, 35, 257–284, doi:10.1146/annurev.ecolsys.35.120202.110122,
688 2004.
- 689 Barnes, C. J. and Allison, G. B.: Tracing of water movement in the unsaturated zone using
690 stable isotopes of hydrogen and oxygen, *J. Hydrol.*, 100(1–3), 143–176, doi:10.1016/0022-
691 1694(88)90184-9, 1988.
- 692 Barthold, F. K., Tyralla, C., Schneider, K., Vaché, K. B., Frede, H.-G. and Breuer, L.: How
693 many tracers do we need for end member mixing analysis (EMMA)? A sensitivity analysis,
694 *Water Resour. Res.*, 47(8), doi:10.1029/2011WR010604, 2011.
- 695 Bertrand, G., Masini, J., Goldscheider, N., Meeks, J., Lavastre, V., Celle-Jeanton, H., Gobat,
696 J.-M. and Hunkeler, D.: Determination of spatiotemporal variability of tree water uptake using
697 stable isotopes ($\delta^{18}\text{O}$, $\delta^2\text{H}$) in an alluvial system supplied by a high-altitude watershed, *Pfyn*
698 *forest, Switzerland, Ecohydrol.*, 7(2), 319–333, doi:10.1002/eco.1347, 2014.
- 699 Blasch, K. W. and Bryson, J. R.: Distinguishing Sources of Ground Water Recharge by Using
700 $\delta^2\text{H}$ and $\delta^{18}\text{O}$, *Ground Water*, 45(3), 294–308, doi:10.1111/j.1745-6584.2006.00289.x, 2007.
- 701 Botter, G., Bertuzzo, E. and Rinaldo, A.: Transport in the hydrologic response: Travel time
702 distributions, soil moisture dynamics, and the old water paradox, *Water Resour. Res.*, 46(3),
703 W03514, doi:10.1029/2009WR008371, 2010.
- 704 Botter, G., Bertuzzo, E. and Rinaldo, A.: Catchment residence and travel time distributions:
705 The master equation, *Geophys. Res. Lett.*, 38(11), L11403, doi:10.1029/2011GL047666, 2011.
- 706 Brodersen, C., Pohl, S., Lindenlaub, M., Leibundgut, C. and Wilpert, K. v: Influence of
707 vegetation structure on isotope content of throughfall and soil water, *Hydrol. Process.*, 14(8),
708 1439–1448, doi:10.1002/1099-1085(20000615)14:8<1439::AID-HYP985>3.0.CO;2-3, 2000.
- 709 Burger, H. M. and Seiler, K. P.: Evaporation from soil water under humid climate conditions
710 and its impact on deuterium and ^{18}O concentrations in groundwater, edited by International
711 Atomic Energy Agency, International Atomic Energy Agency, Vienna, Austria., 1992.
- 712 Buttle, J. M.: Isotope hydrograph separations and rapid delivery of pre-event water from
713 drainage basins, *Prog. Phys. Geogr.*, 18(1), 16–41, doi:10.1177/030913339401800102, 1994.
- 714 Buttle, J. M.: Isotope Hydrograph Separation of Runoff Sources, in *Encyclopedia of*
715 *Hydrological Sciences*, edited by M. G. Anderson, p. 10:116, John Wiley & Sons, Ltd,
716 Chichester, Great Britain., 2006.
- 717 Buttle, J. M. and McDonald, D. J.: Coupled vertical and lateral preferential flow on a forested
718 slope, *Water Resour. Res.*, 38(5), 18–1, doi:10.1029/2001WR000773, 2002.
- 719 Clark, I. D. and Fritz, P.: Groundwater, in *Environmental Isotopes in Hydrogeology*, p. 80, CRC
720 Press, Florida, FL, USA., 1997a.
- 721 Clark, I. D. and Fritz, P.: Methods for Field Sampling, in *Environmental Isotopes in*
722 *Hydrogeology*, p. 283, CRC Press, Florida, FL, USA., 1997b.

- 723 Clark, I. D. and Fritz, P.: The Environmental Isotopes, in Environmental Isotopes in
724 Hydrogeology, pp. 2–34, CRC Press, Florida, FL, USA., 1997c.
- 725 Cooper, L. W.: Isotopic Fractionation in Snow Cover, in Isotope Tracers in Catchment
726 Hydrology, edited by C. Kendall and J. J. McDonnell, pp. 119–136, Elsevier, Amsterdam,
727 Netherlands., 1998.
- 728 Craig, H.: Isotopic Variations in Meteoric Waters, *Science*, 133(3465), 1702–1703,
729 doi:10.1126/science.133.3465.1702, 1961a.
- 730 Craig, H.: Standard for reporting concentrations of deuterium and oxygen-18 in natural waters,
731 *Science*, 133(3467), 1833, 1961b.
- 732 Csardi, G. and Nepusz, T.: The igraph software package for complex network research,
733 *Complex Systems* 1695. [online] Available from: <http://igraph.sf.net> (Accessed 24 December
734 2015), 2006.
- 735 Dansgaard, W.: Stable isotopes in precipitation, *Tellus*, 16(4), 436–468, doi:10.1111/j.2153-
736 3490.1964.tb00181.x, 1964.
- 737 Darling, W. G.: Hydrological factors in the interpretation of stable isotopic proxy data present
738 and past: a European perspective, *Quat. Sci. Rev.*, 23(7–8), 743–770,
739 doi:10.1016/j.quascirev.2003.06.016, 2004.
- 740 Duvert, C., Stewart, M. K., Cendón, D. I. and Raiber, M.: Time series of tritium, stable isotopes
741 and chloride reveal short-term variations in groundwater contribution to a stream, *Hydrol. Earth
742 Syst. Sci.*, 20(1), 257–277, doi:10.5194/hess-20-257-2016, 2016.
- 743 DWD: Deutscher Wetterdienst - Wetter und Klima, Bundesministerium für Verkehr und
744 digitale Infrastruktur, [online] Available from: <http://dwd.de/> (Accessed 17 February 2014),
745 2014.
- 746 Foerstel, H., Frinken, J., Huetzen, H., Lembrich, D. and Puetz, T.: Application of H₂¹⁸O as a
747 tracer of water flow in soil, International Atomic Energy Agency, Vienna, Austria., 1991.
- 748 Garvelmann, J., Kuells, C. and Weiler, M.: A porewater-based stable isotope approach for the
749 investigation of subsurface hydrological processes, *Hydrol. Earth Syst. Sci.*, 16(2), 631–640,
750 doi:10.5194/hess-16-631-2012, 2012.
- 751 Gat, J. R.: Oxygen and Hydrogen Isotopes in the Hydrologic Cycle, *Annu. Rev. Earth Planet.
752 Sci.*, 24(1), 225–262, doi:10.1146/annurev.earth.24.1.225, 1996.
- 753 Gat, J., R., Mook, W. G. and Meijer, H. A. J.: Environmental isotopes in the hydrological cycle:
754 Principles and Applications, edited by W. G. Mook, International Hydrological Programme;
755 United Nations Educational, Scientific and Cultural Organization and International Atomic
756 Energy Agency, Paris, France., 2001.
- 757 Gehrels, J. C., Peeters, J. E. M., de Vries, J. J. and Dekkers, M.: The mechanism of soil water
758 movement as inferred from ¹⁸O stable isotope studies, *Hydrol. Sci. J.*, 43(4), 579–594,
759 doi:10.1080/02626669809492154, 1998.
- 760 Genereux, D. P. and Hooper, R. P.: Oxygen and Hydrogen Isotopes in Rainfall-Runoff Studies,
761 in Isotope Tracers in Catchment Hydrology, edited by C. Kendall and J. J. McDonnell, pp. 319–
762 346, Elsevier, Amsterdam, Netherlands., 1998.
- 763 Geris, J., Tetzlaff, D., McDonnell, J. and Soulsby, C.: The relative role of soil type and tree
764 cover on water storage and transmission in northern headwater catchments, *Hydrol. Process.*,
765 29(7), 1844–1860, doi:10.1002/hyp.10289, 2015.

- 766 Gomez, J. D. and Wilson, J. L.: Age distributions and dynamically changing hydrologic
767 systems: Exploring topography-driven flow, *Water Resour. Res.*, 49(3), 1503–1522,
768 doi:10.1002/wrcr.20127, 2013.
- 769 Gonfiantini, R., Fröhlich, K., Araguás-Araguás, L. and Rozanski, K.: Isotopes in Groundwater
770 Hydrology, in *Isotope Tracers in Catchment Hydrology*, edited by C. Kendall and J. J.
771 McDonnell, pp. 203–246, Elsevier, Amsterdam, Netherlands., 1998.
- 772 Gordon, L. J., Finlayson, C. M. and Falkenmark, M.: Managing water in agriculture for food
773 production and other ecosystem services, *Agric. Water Manag.*, 97(4), 512–519,
774 doi:10.1016/j.agwat.2009.03.017, 2010.
- 775 Harman, C. J.: Time-variable transit time distributions and transport: Theory and application to
776 storage-dependent transport of chloride in a watershed, *Water Resour. Res.*, 51(1), 1–30,
777 doi:10.1002/2014WR015707, 2015.
- 778 Heidebüchel, I., Troch, P. A., Lyon, S. W. and Weiler, M.: The master transit time distribution
779 of variable flow systems, *Water Resour. Res.*, 48(6), W06520, doi:10.1029/2011WR011293,
780 2012.
- 781 Hindmarsh, A. C., Brown, P. N., Grant, K. E., Lee, S. L., Serban, R., Shumaker, D. E. and
782 Woodward, C. S.: SUNDIALS: Suite of Nonlinear and Differential/Algebraic Equation
783 Solvers, *ACM Trans. Math. Softw.*, 31(3), 363–396, doi:10.1145/1089014.1089020, 2005.
- 784 Hollander, M., Wolfe, D. A. and Chicken, E.: *Nonparametric Statistical Methods*, John Wiley
785 & Sons, New York, NY, USA., 2013.
- 786 Hrachowitz, M., Benettin, P., van Breukelen, B. M., Fovet, O., Howden, N. J. K., Ruiz, L., van
787 der Velde, Y. and Wade, A. J.: Transit times—the link between hydrology and water quality at
788 the catchment scale, *Wiley Interdiscip. Rev. Water*, doi:10.1002/wat2.1155, 2016.
- 789 IAEA: International Atomic Energy Agency: Water Resources Programme – Global Network
790 of Isotopes in Precipitation, [online] Available from: [http://www-](http://www-naweb.iaea.org/naweb/ih/IHS_resources_gnip.html)
791 [naweb.iaea.org/naweb/ih/IHS_resources_gnip.html](http://www-naweb.iaea.org/naweb/ih/IHS_resources_gnip.html) (Accessed 11 August 2014), 2014.
- 792 Jin, L., Siegel, D. I., Lautz, L. K., Mitchell, M. J., Dahms, D. E. and Mayer, B.: Calcite
793 precipitation driven by the common ion effect during groundwater–surface-water mixing: A
794 potentially common process in streams with geologic settings containing gypsum, *Geol. Soc.
795 Am. Bull.*, 122(7/8), B30011.1, doi:10.1130/B30011.1, 2010.
- 796 Jin, L., Siegel, D. I., Lautz, L. K. and Lu, Z.: Identifying streamflow sources during spring
797 snowmelt using water chemistry and isotopic composition in semi-arid mountain streams, *J.
798 Hydrol.*, 470–471, 289–301, doi:10.1016/j.jhydrol.2012.09.009, 2012.
- 799 Jouzel, J., Alley, R. B., Cuffey, K. M., Dansgaard, W., Grootes, P., Hoffmann, G., Johnsen, S.
800 J., Koster, R. D., Peel, D., Shuman, C. A., Stievenard, M., Stuiver, M. and White, J.: Validity
801 of the temperature reconstruction from water isotopes in ice cores, *J. Geophys. Res.*, 102,
802 26471–26487, doi:10.1029/97JC01283, 1997.
- 803 Kendall, C. and Caldwell, E. A.: Fundamentals of Isotope Geochemistry, in *Isotope Tracers in
804 Catchment Hydrology*, edited by C. Kendall and J. J. McDonnell, pp. 51–86, Elsevier,
805 Amsterdam, Netherlands., 1998.
- 806 Kirchner, J. W.: A double paradox in catchment hydrology and geochemistry, *Hydrol. Process.*,
807 17(4), 871–874, doi:10.1002/hyp.5108, 2003.
- 808 Klaus, J., McDonnell, J. J., Jackson, C. R., Du, E. and Griffiths, N. A.: Where does streamwater

809 come from in low-relief forested watersheds? A dual-isotope approach, *Hydrol. Earth Syst.*
810 *Sci.*, 19(1), 125–135, 2015.

811 Koeniger, P., Leibundgut, C. and Stichler, W.: Spatial and temporal characterisation of stable
812 isotopes in river water as indicators of groundwater contribution and confirmation of modelling
813 results; a study of the Weser river, Germany, *Isotopes Environ. Health Stud.*, 45(4), 289–302,
814 doi:10.1080/10256010903356953, 2009.

815 Kolaczyk, E. D.: *Statistical Analysis of Network Data with R*, Springer Science & Business
816 Media, New York, NY, USA., 2014.

817 Kortelainen, N. M. and Karhu, J. A.: Regional and seasonal trends in the oxygen and hydrogen
818 isotope ratios of Finnish groundwaters: a key for mean annual precipitation, *J. Hydrol.*, 285(1–
819 4), 143–157, doi:10.1016/j.jhydrol.2003.08.014, 2004.

820 Kraft, P., Vaché, K. B., Frede, H.-G. and Breuer, L.: CMF: A Hydrological Programming
821 Language Extension For Integrated Catchment Models, *Environ. Model. Softw.*, 26(6), 828–
822 830, doi:10.1016/j.envsoft.2010.12.009, 2011.

823 Lai, C.-T. and Ehleringer, J. R.: Deuterium excess reveals diurnal sources of water vapor in
824 forest air, *Oecologia*, 165(1), 213–223, doi:10.1007/s00442-010-1721-2, 2011.

825 Lauer, F., Frede, H.-G. and Breuer, L.: Uncertainty assessment of quantifying spatially
826 concentrated groundwater discharge to small streams by distributed temperature sensing, *Water*
827 *Resour. Res.*, 49(1), 400–407, doi:10.1029/2012WR012537, 2013.

828 LGR: Los Gatos Research, Greenhouse Gas, isotope and trace gas analyzers, [online] Available
829 from: <http://www.lgrinc.com/> (Accessed 5 February 2013), 2013.

830 Li, F., Song, X., Tang, C., Liu, C., Yu, J. and Zhang, W.: Tracing infiltration and recharge using
831 stable isotope in Taihang Mt., North China, *Environ. Geol.*, 53(3), 687–696,
832 doi:10.1007/s00254-007-0683-0, 2007.

833 Maloszewski, P. and Zuber, A.: Manual on lumped parameter models used for the interpretation
834 of environmental tracer data in groundwaters, in *Use of isotopes for analyses of flow and*
835 *transport dynamics in groundwater systems*, p. 50, International Atomic Energy Agency,
836 Vienna, Austria., 2002.

837 McConville, C., Kalin, R. m., Johnston, H. and McNeill, G. w.: Evaluation of Recharge in a
838 Small Temperate Catchment Using Natural and Applied $\delta^{18}\text{O}$ Profiles in the Unsaturated Zone,
839 *Ground Water*, 39(4), 616–623, doi:10.1111/j.1745-6584.2001.tb02349.x, 2001.

840 McDonnell, J. J. and Beven, K.: Debates—The future of hydrological sciences: A (common)
841 path forward? A call to action aimed at understanding velocities, celerities and residence time
842 distributions of the headwater hydrograph, *Water Resour. Res.*, 50(6), 5342–5350,
843 doi:10.1002/2013WR015141, 2014.

844 McDonnell, J. J., Sivapalan, M., Vaché, K., Dunn, S., Grant, G., Haggerty, R., Hinz, C., Hooper,
845 R., Kirchner, J., Roderick, M. L. and others: Moving beyond heterogeneity and process
846 complexity: a new vision for watershed hydrology, *Water Resour. Res.*, 43(7), W07301, 2007.

847 McDonnell, J. J., McGuire, K., Aggarwal, P., Beven, K. J., Biondi, D., Destouni, G., Dunn, S.,
848 James, A., Kirchner, J., Kraft, P., Lyon, S., Maloszewski, P., Newman, B., Pfister, L., Rinaldo,
849 A., Rodhe, A., Sayama, T., Seibert, J., Solomon, K., Soulsby, C., Stewart, M., Tetzlaff, D.,
850 Tobin, C., Troch, P., Weiler, M., Western, A., Worman, A. and Wrede, S.: How old is
851 streamwater? Open questions in catchment transit time conceptualization, modelling and
852 analysis, *Hydrol. Process.*, 24(12), 1745–1754, 2010.

- 853 McGuire, K. J. and McDonnell, J. J.: A review and evaluation of catchment transit time
854 modeling, *J. Hydrol.*, 330(3), 543–563, 2006.
- 855 Michel, R. L.: Residence times in river basins as determined by analysis of long-term tritium
856 records, *J. Hydrol.*, 130(1), 367–378, doi:10.1016/0022-1694(92)90117-E, 1992.
- 857 Mook, W. G., Groeneveld, D. J., Brouwn, A. E. and Ganswijk, A. J. van: Analysis of a run-off
858 hydrograph by means of natural ^{18}O , in *Isotope techniques in groundwater hydrology*, vol. 1,
859 pp. 159–169, International Atomic Energy Agency, Vienna, Austria., 1974.
- 860 Muñoz-Villers, L. E. and McDonnell, J. J.: Runoff generation in a steep, tropical montane cloud
861 forest catchment on permeable volcanic substrate, *Water Resour. Res.*, 48(9), n/a–n/a,
862 doi:10.1029/2011WR011316, 2012.
- 863 Neal, C. and Rosier, P. T. W.: Chemical studies of chloride and stable oxygen isotopes in two
864 conifer afforested and moorland sites in the British uplands, *J. Hydrol.*, 115(1–4), 269–283,
865 doi:10.1016/0022-1694(90)90209-G, 1990.
- 866 Newman, B., Tanweer, A. and Kurttas, T.: IAEA Standard Operating Procedure for the Liquid-
867 Water Stable Isotope Analyser, *Laser Proced. IAEA Water Resour. Programme*, 2009.
- 868 O’Driscoll, M. A., DeWalle, D. R., McGuire, K. J. and Gburek, W. J.: Seasonal ^{18}O variations
869 and groundwater recharge for three landscape types in central Pennsylvania, USA, *J. Hydrol.*,
870 303(1–4), 108–124, doi:10.1016/j.jhydrol.2004.08.020, 2005.
- 871 Orłowski, N., Frede, H.-G., Brüggemann, N. and Breuer, L.: Validation and application of a
872 cryogenic vacuum extraction system for soil and plant water extraction for isotope analysis, *J.*
873 *Sens. Sens. Syst.*, 2(2), 179–193, doi:10.5194/jsss-2-179-2013, 2013.
- 874 Orłowski, N., Lauer, F., Kraft, P., Frede, H.-G. and Breuer, L.: Linking Spatial Patterns of
875 Groundwater Table Dynamics and Streamflow Generation Processes in a Small Developed
876 Catchment, *Water*, 6(10), 3085–3117, doi:10.3390/w6103085, 2014.
- 877 Penna, D., Ahmad, M., Birks, S. J., Bouchaou, L., Brenčič, M., Butt, S., Holko, L., Jeelani, G.,
878 Martínez, D. E., Melikadze, G., Shanley, J. B., Sokratov, S. A., Stadnyk, T., Sugimoto, A. and
879 Vreča, P.: A new method of snowmelt sampling for water stable isotopes, *Hydrol. Process.*,
880 28(22), 5637–5644, doi:10.1002/hyp.10273, 2014.
- 881 Peralta-Tapia, A., Sponseller, R. A., Tetzlaff, D., Soulsby, C. and Laudon, H.: Connecting
882 precipitation inputs and soil flow pathways to stream water in contrasting boreal catchments,
883 *Hydrol. Process.*, 29(16), 3546–3555, doi:10.1002/hyp.10300, 2015.
- 884 Perry, C. and Taylor, K.: *Environmental Sedimentology*, p. 36, Blackwell Publishing, Oxford,
885 OX, UK, 2009.
- 886 Pierce, S. C., Kröger, R. and Pezeshki, R.: Managing Artificially Drained Low-Gradient
887 Agricultural Headwaters for Enhanced Ecosystem Functions, *Biology*, 1(3), 794–856,
888 doi:10.3390/biology1030794, 2012.
- 889 Qu, Y. and Duffy, C. J.: A semidiscrete finite volume formulation for multiprocess watershed
890 simulation, *Water Resour. Res.*, 43(8), W08419, doi:10.1029/2006WR005752, 2007.
- 891 Rinaldo, A., Benettin, P., Harman, C. J., Hrachowitz, M., McGuire, K. J., van der Velde, Y.,
892 Bertuzzo, E. and Botter, G.: Storage selection functions: A coherent framework for quantifying
893 how catchments store and release water and solutes, *Water Resour. Res.*, 51(6), 4840–4847,
894 doi:10.1002/2015WR017273, 2015.
- 895 Rohde, A.: Snowmelt-Dominated Systems, in *Isotope Tracers in Catchment Hydrology*, edited

- 896 by C. Kendall and J. J. McDonnell, pp. 391–433, Elsevier, Amsterdam, Netherlands., 1998.
- 897 Rozanski, K., Sonntag, C. and Münnich, K. O.: Factors controlling stable isotope composition
898 of European precipitation, *Tellus*, 34(2), 142–150, doi:10.1111/j.2153-3490.1982.tb01801.x,
899 1982.
- 900 Rozanski, K., Froehlich, K. and Mook, W. G.: in *Environmental isotopes in the hydrological*
901 *cycle: Principles and Applications*, vol. 3, International Hydrological Programme; United
902 Nations Educational, Scientific and Cultural Organization and International Atomic Energy
903 Agency, Paris, Vienna., 2001.
- 904 Schultz, N. M., Griffis, T. J., Lee, X. and Baker, J. M.: Identification and correction of spectral
905 contamination in $^2\text{H}/^1\text{H}$ and $^{18}\text{O}/^{16}\text{O}$ measured in leaf, stem, and soil water, *Rapid Commun.*
906 *Mass Spectrom.*, 25(21), 3360–3368, doi:10.1002/rcm.5236, 2011.
- 907 Shuttleworth, W. J. and Wallace, J. S.: Evaporation from sparse crops-an energy combination
908 theory, *Q. J. R. Meteorol. Soc.*, 111(469), 839–855, doi:10.1002/qj.49711146910, 1985.
- 909 Sklash, M. G.: Environmental isotope studies of storm and snowmelt runoff generation, in
910 *Process studies in hillslope hydrology*, edited by M. G. Anderson, pp. 410–435, Wiley, New
911 York, NY, USA., 1990.
- 912 Sklash, M. G. and Farvolden, R. N.: The Role Of Groundwater In Storm Runoff, in
913 *Developments in Water Science*, vol. 12, edited by W. B. and D. A. Stephenson, pp. 45–65,
914 Elsevier, Amsterdam, Netherlands., 1979.
- 915 Song, X., Wang, P., Yu, J., Liu, X., Liu, J. and Yuan, R.: Relationships between precipitation,
916 soil water and groundwater at Chongling catchment with the typical vegetation cover in the
917 Taihang mountainous region, China, *Environ. Earth Sci.*, 62(4), 787–796, doi:10.1007/s12665-
918 010-0566-7, 2011.
- 919 Sprenger, M., Erhardt, M., Riedel, M. and Weiler, M.: Historical tracking of nitrate in
920 contrasting vineyards using water isotopes and nitrate depth profiles, *Agric. Ecosyst. Environ.*,
921 222, 185–192, doi:10.1016/j.agee.2016.02.014, 2016a.
- 922 Sprenger, M., Seeger, S., Blume, T. and Weiler, M.: Travel times in the vadose zone: Variability
923 in space and time, *Water Resour. Res.*, n/a-n/a, doi:10.1002/2015WR018077, 2016b.
- 924 Stewart, M. K., Morgenstern, U. and McDonnell, J. J.: Truncation of stream residence time:
925 how the use of stable isotopes has skewed our concept of streamwater age and origin, *Hydrol.*
926 *Process.*, 24(12), 1646–1659, doi:10.1002/hyp.7576, 2010.
- 927 Stumpp, C. and Hendry, M. J.: Spatial and temporal dynamics of water flow and solute transport
928 in a heterogeneous glacial till: The application of high-resolution profiles of $\delta^{18}\text{O}$ and $\delta^2\text{H}$ in
929 pore waters, *J. Hydrol.*, 438–439, 203–214, doi:10.1016/j.jhydrol.2012.03.024, 2012.
- 930 Stumpp, C., Klaus, J. and Stichler, W.: Analysis of long-term stable isotopic composition in
931 German precipitation, *J. Hydrol.*, 517, 351–361, doi:10.1016/j.jhydrol.2014.05.034, 2014.
- 932 Tang, K. and Feng, X.: The effect of soil hydrology on the oxygen and hydrogen isotopic
933 compositions of plants' source water, *Earth Planet. Sci. Lett.*, 185(3–4), 355–367, 2001.
- 934 Taylor, S., Feng, X., Kirchner, J. W., Osterhuber, R., Klaue, B. and Renshaw, C. E.: Isotopic
935 evolution of a seasonal snowpack and its melt, *Water Resour. Res.*, 37(3), 759–769,
936 doi:10.1029/2000WR900341, 2001.
- 937 Thomas, E. M., Lin, H., Duffy, C. J., Sullivan, P. L., Holmes, G. H., Brantley, S. L. and Jin, L.:
938 Spatiotemporal Patterns of Water Stable Isotope Compositions at the Shale Hills Critical Zone

939 Observatory: Linkages to Subsurface Hydrologic Processes, *Vadose Zone J.*, 12(4), 0,
940 doi:10.2136/vzj2013.01.0029, 2013.

941 Timbe, E., Windhorst, D., Crespo, P., Frede, H.-G., Feyen, J. and Breuer, L.: Understanding
942 uncertainties when inferring mean transit times of water through tracer-based lumped-parameter
943 models in Andean tropical montane cloud forest catchments, *Hydrol. Earth Syst. Sci.*, 18(4),
944 1503–1523, doi:10.5194/hess-18-1503-2014, 2014.

945 van der Velde, Y., Torfs, P. J. J. F., van der Zee, S. E. a. T. M. and Uijlenhoet, R.: Quantifying
946 catchment-scale mixing and its effect on time-varying travel time distributions, *Water Resour.*
947 *Res.*, 48(6), W06536, doi:10.1029/2011WR011310, 2012.

948 Wang, P., Song, X., Han, D., Zhang, Y. and Liu, X.: A study of root water uptake of crops
949 indicated by hydrogen and oxygen stable isotopes: A case in Shanxi Province, China, *Agric.*
950 *Water Manag.*, 97(3), 475–482, 2010.

951 Wang, X. F. and Yakir, D.: Using stable isotopes of water in evapotranspiration studies, *Hydrol.*
952 *Process.*, 14(8), 1407–1421, doi:10.1002/1099-1085(20000615)14:8<1407::AID-
953 HYP992>3.0.CO;2-K, 2000.

954 Windhorst, D., Waltz, T., Timbe, E., Frede, H.-G. and Breuer, L.: Impact of elevation and
955 weather patterns on the isotopic composition of precipitation in a tropical montane rainforest,
956 *Hydrol. Earth Syst. Sci.*, 17(1), 409–419, doi:10.5194/hess-17-409-2013, 2013.

957 Windhorst, D., Kraft, P., Timbe, E., Frede, H.-G. and Breuer, L.: Stable water isotope tracing
958 through hydrological models for disentangling runoff generation processes at the hillslope
959 scale, *Hydrol. Earth Syst. Sci.*, 18(10), 4113–4127, doi:10.5194/hess-18-4113-2014, 2014.

960 Woolfenden, L. R. and Ginn, T. R.: Modeled Ground Water Age Distributions, *Ground Water*,
961 47(4), 547–557, doi:10.1111/j.1745-6584.2008.00550.x, 2009.

962 Wu, J., Ding, Y., Ye, B., Yang, Q., Hou, D. and Xue, L.: Stable isotopes in precipitation in
963 Xilin River Basin, northern China and their implications, *Chin. Geogr. Sci.*, 22(5), 531–540,
964 doi:10.1007/s11769-012-0543-z, 2012.

965 Xia, Y.: Optimization and uncertainty estimates of WMO regression models for the systematic
966 bias adjustment of NLDAS precipitation in the United States, *J. Geophys. Res. Atmospheres*,
967 111(D8), D08102, doi:10.1029/2005JD006188, 2006.

968 Yurtsever, Y.: Worldwide survey of stable isotopes in precipitation, International Atomic
969 Energy Agency, Vienna, Austria., 1975.

970 Zhao, L., Xiao, H., Zhou, J., Wang, L., Cheng, G., Zhou, M., Yin, L. and McCabe, M. F.:
971 Detailed assessment of isotope ratio infrared spectroscopy and isotope ratio mass spectrometry
972 for the stable isotope analysis of plant and soil waters, *Rapid Commun. Mass Spectrom.*, 25(20),
973 3071–3082, doi:10.1002/rcm.5204, 2011.

974

975 Table 1. Descriptive statistics of $\delta^2\text{H}$, $\delta^{18}\text{O}$, and d-excess values for precipitation, stream, and
 976 groundwater over the two-year observation period including all sampling points.

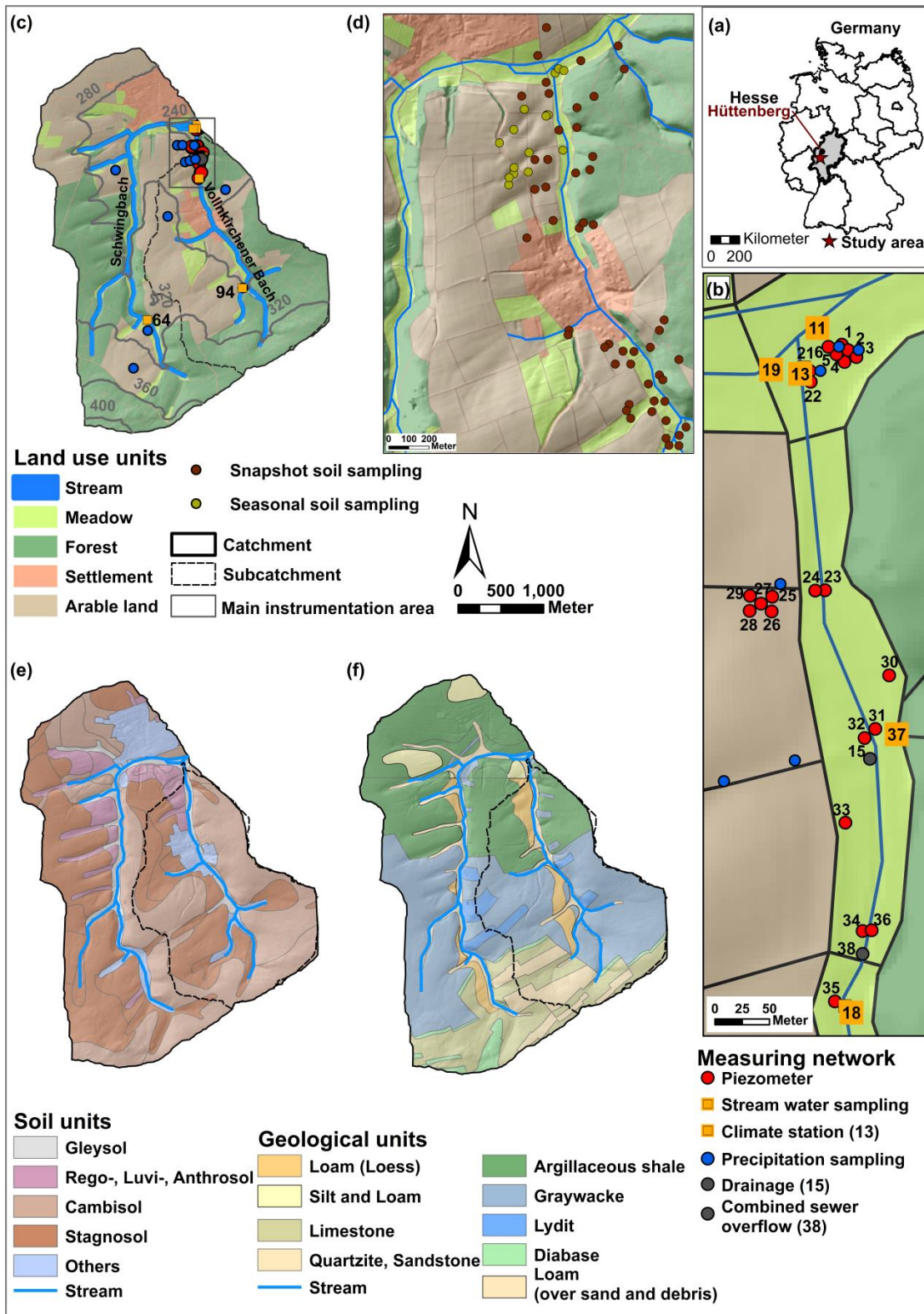
Sample type	Mean \pm SD		Min		Max		D-excess mean \pm SD	N
	$\delta^2\text{H}$	$\delta^{18}\text{O}$	$\delta^2\text{H}$	$\delta^{18}\text{O}$	$\delta^2\text{H}$	$\delta^{18}\text{O}$		
	[‰]	[‰]	[‰]	[‰]	[‰]	[‰]		
Precipitation	-43.9 \pm 23.4	-6.2 \pm 3.1	-167.6	-22.4	-8.3	-1.2	5.9 \pm 5.7	592
Vollnkirchener Bach	-58.0 \pm 2.8	-8.4 \pm 0.4	-66.3	-10.0	-26.9	-6.7	9.0 \pm 2.3	332
Schwingbach	-58.2 \pm 4.3	-8.4 \pm 0.6	-139.7	-18.3	-47.2	-5.9	9.0 \pm 2.2	463
Groundwater meadow	-57.6 \pm 1.6	-8.2 \pm 0.4	-64.9	-9.2	-50.8	-5.7	7.9 \pm 5.5	375
Groundwater arable land	-56.2 \pm 3.7	-8.0 \pm 0.5	-91.6	-12.3	-49.5	-6.8	1.7 \pm 5.0	338
Groundwater along stream	-59.9 \pm 6.8	-8.5 \pm 0.9	-94.5	-13.0	-49.5	-7.0	8.2 \pm 1.5	108

977

978 Table 2. Mean and standard deviation (SD) for isotopic signatures and soil physical properties in 0.2 m and 0.5 m soil depth (N=52 per depth).

	$\delta^2\text{H}$ [‰]		$\delta^{18}\text{O}$ [‰]		water content [% w/w]		pH		bulk density [g cm ⁻³]	
	0.2 m	0.5 m	0.2 m	0.5 m	0.2 m	0.5 m	0.2 m	0.5 m	0.2 m	0.5 m
Mean±SD	-46.9±8.4	-58.5±8.3	-6.6±1.2	-8.2±1.2	16.8±7.2	16.1±8.3	5.0±1.0	5.3±1.0	1.3±0.2	1.3±0.2

979



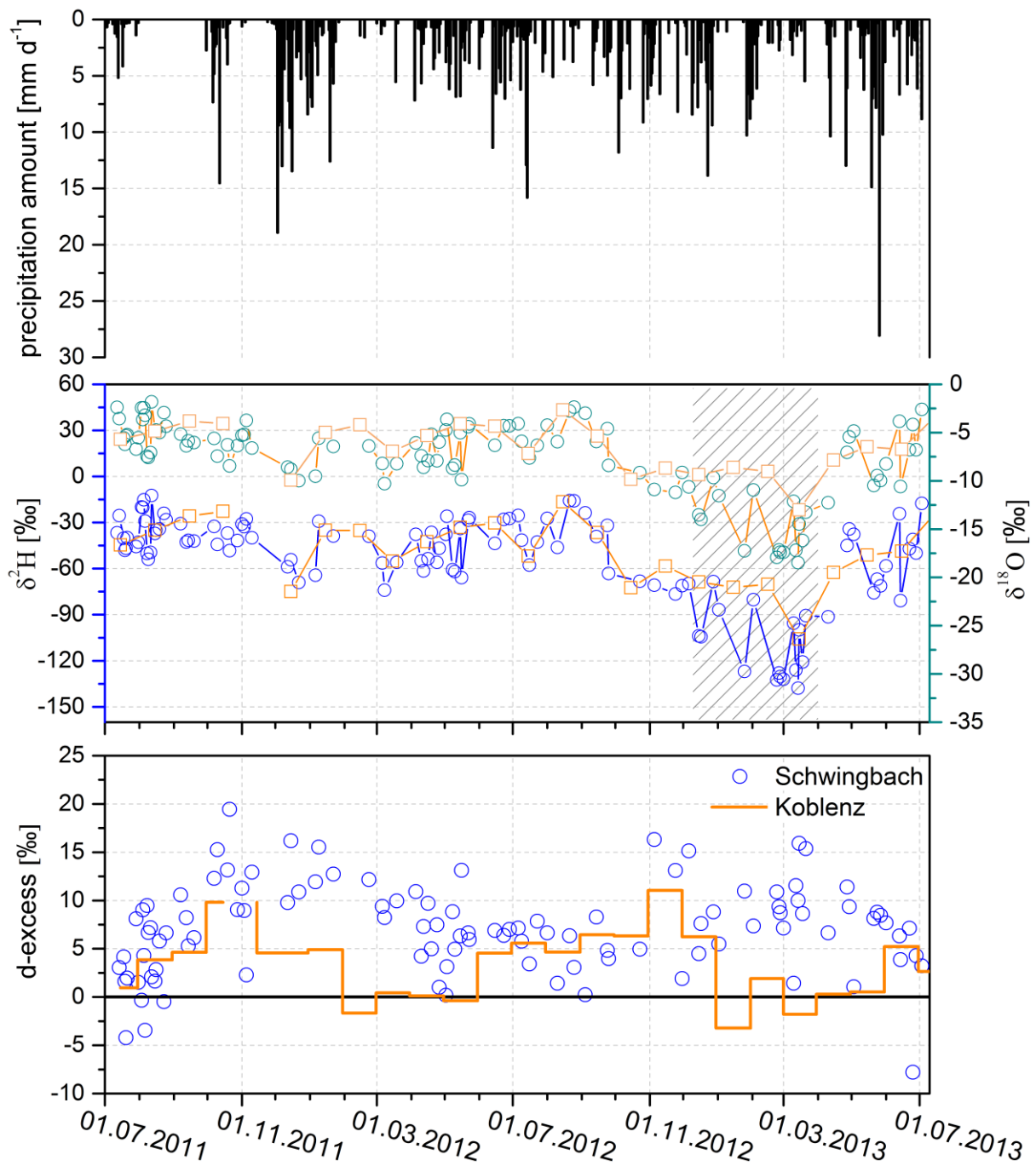
980

981

982 Figure 1. Maps show (a) the location of the Schwingbach catchment in Germany, (b) the main

983 monitoring area, (c) the land use, elevation, and instrumentation, (d) the locations of the

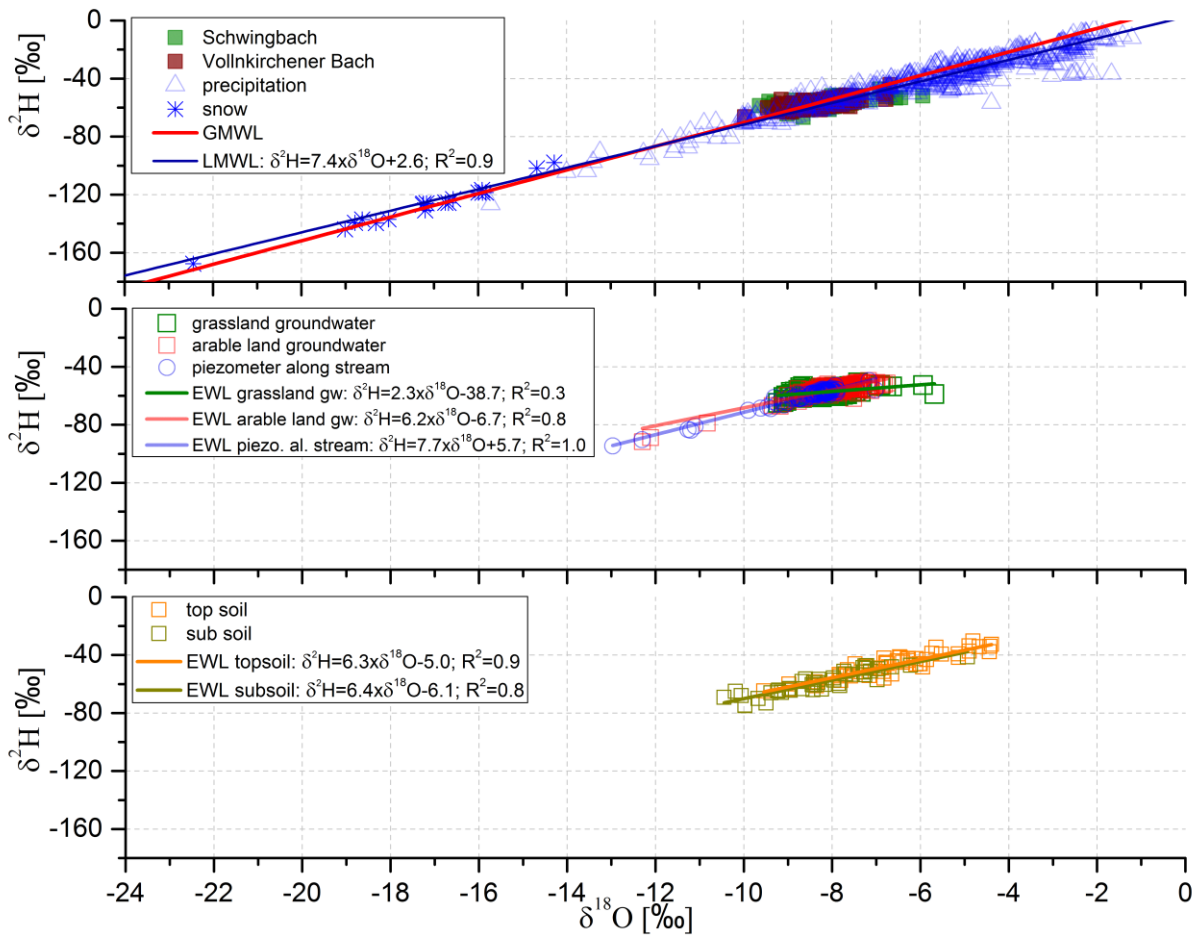
984 snapshot as well as the seasonal soil samplings, (e) soil types, and (f) geology of the
985 Schwingbach catchment including the Vollnkirchener Bach subcatchment boudaries.
986



987

988

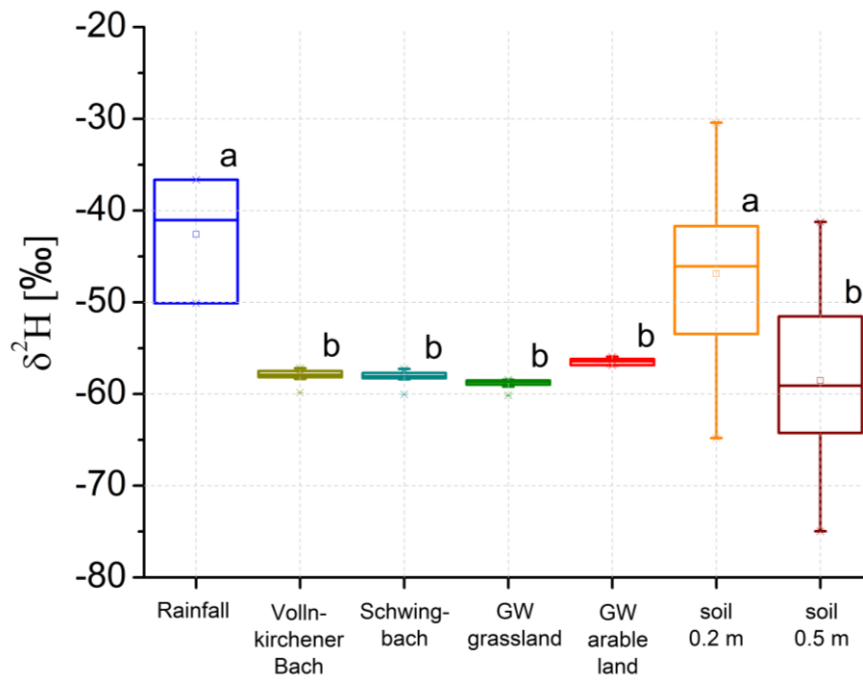
989 Figure 2. Temporal variation of precipitation amount, isotopic signatures ($\delta^2\text{H}$ and $\delta^{18}\text{O}$)
 990 including snow samples (grey striped box) of the Schwingbach and GNIP station Koblenz, and
 991 d-excess values for the study area compared to monthly d-excess values (July 2011 to July
 992 2013) of GNIP station Koblenz with reference d-excess of GMWL ($d=10$; solid black line).
 993



994

995

996 Figure 3. Local Meteoric Water Line for the Schwingbach catchment (LMWL) in comparison
 997 to GMWL, including comparisons between precipitation, stream water, groundwater, and soil
 998 water isotopic signatures and the respective EWLs.

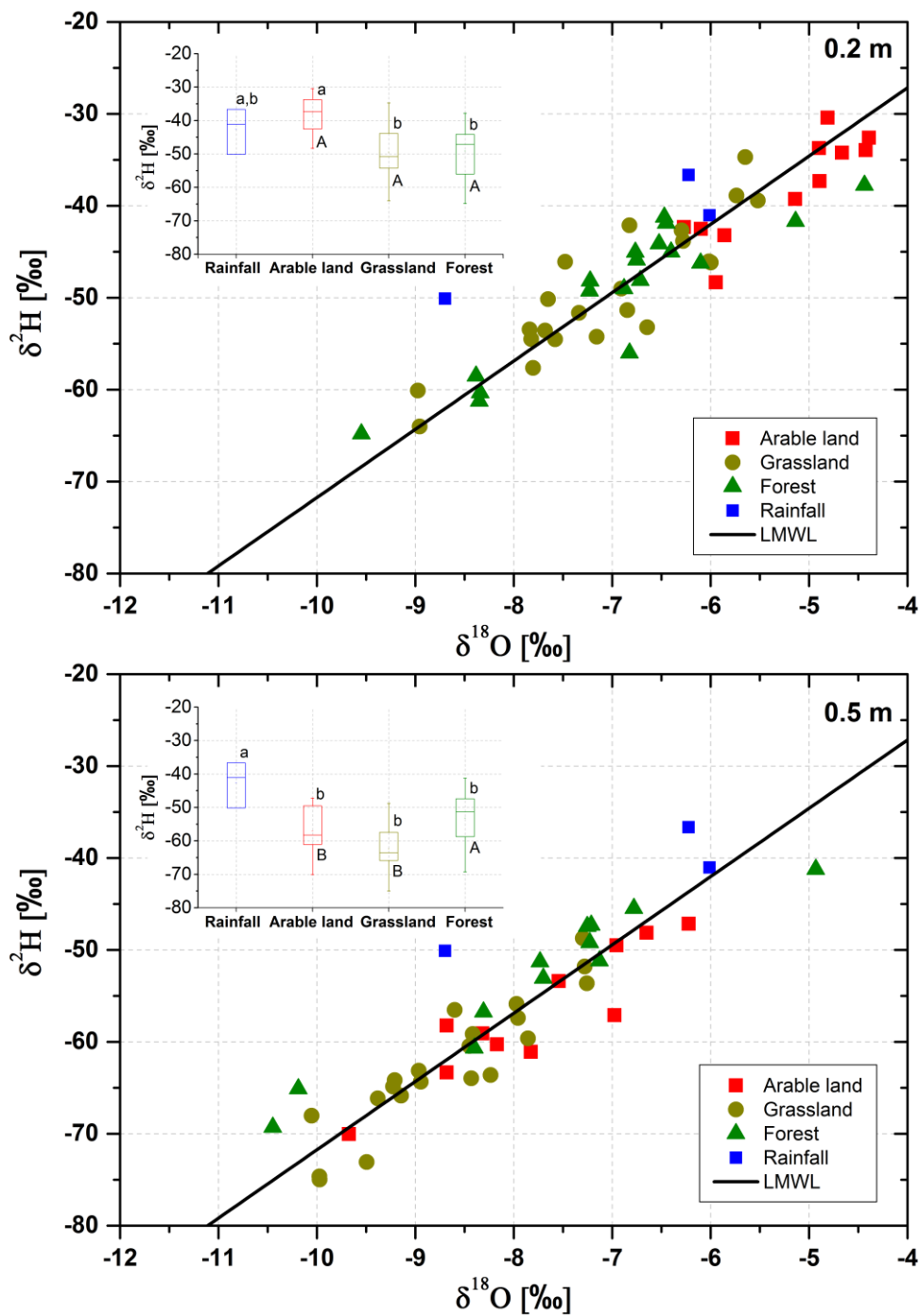


999

1000

1001 Figure 4. Boxplots of $\delta^2\text{H}$ values comparing precipitation, stream, groundwater, and soil
 1002 isotopic composition in 0.2 m and 0.5 m depth (N=52 per depth). Different letters indicate
 1003 significant differences ($p \leq 0.05$).

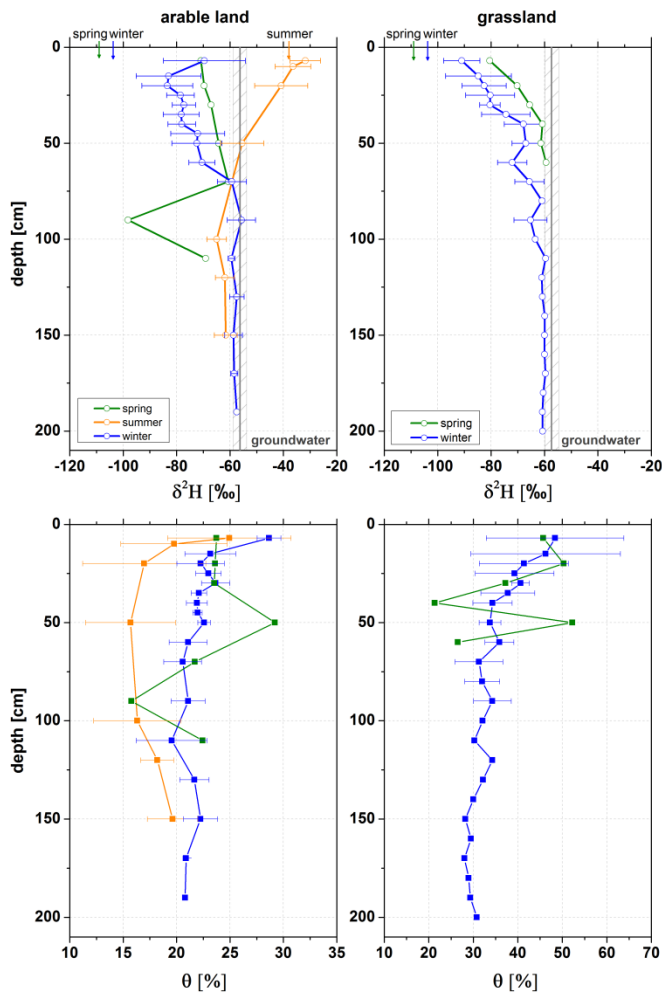
1004



1005

1006

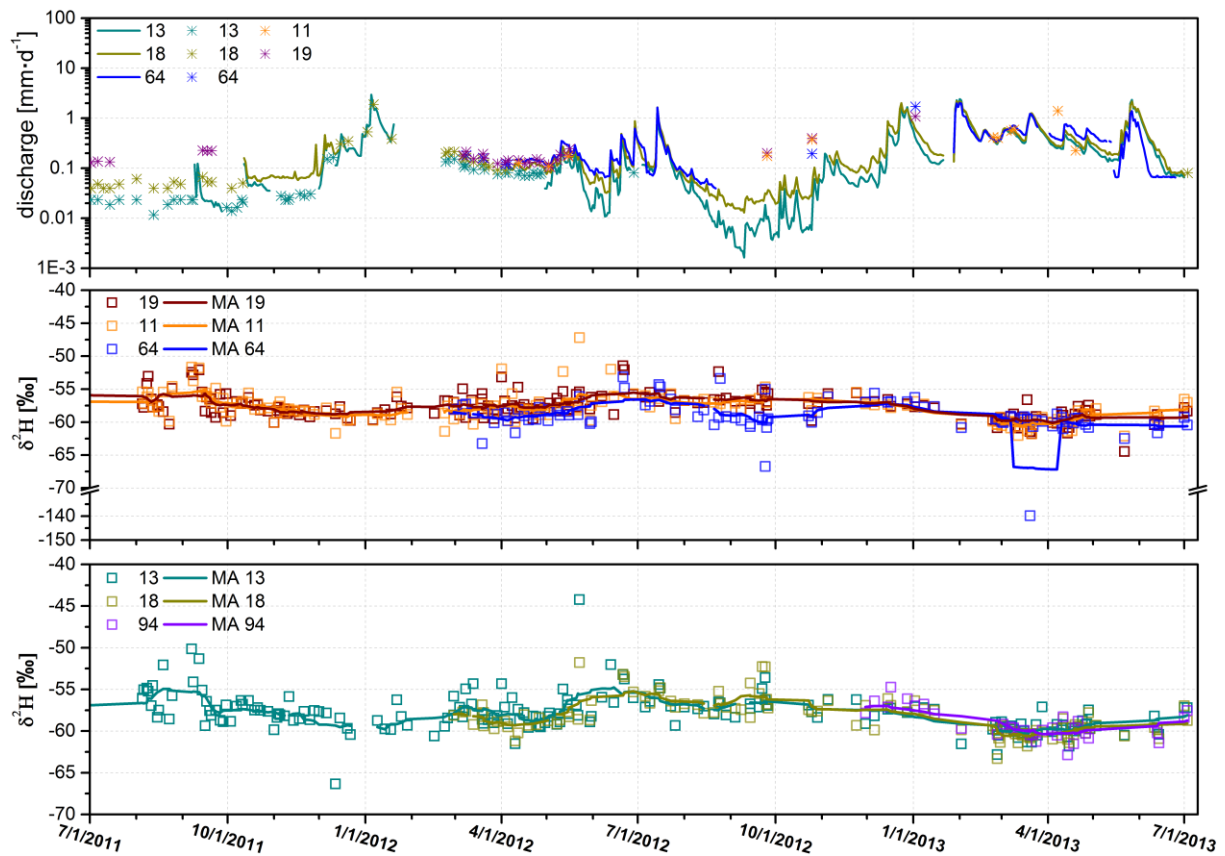
1007 Figure 5. Dual isotope plot of soil water isotopic signatures in 0.2 m and 0.5 m depth compared
 1008 by land use including precipitation isotope data from 19, 21, and 28 October 2011. Insets:
 1009 Boxplots comparing $\delta^2\text{H}$ isotopic signatures between different land use units and precipitation
 1010 (small letters) in top and subsoil (capital letters). Different letters indicate significant
 1011 differences ($p \leq 0.05$).



1012

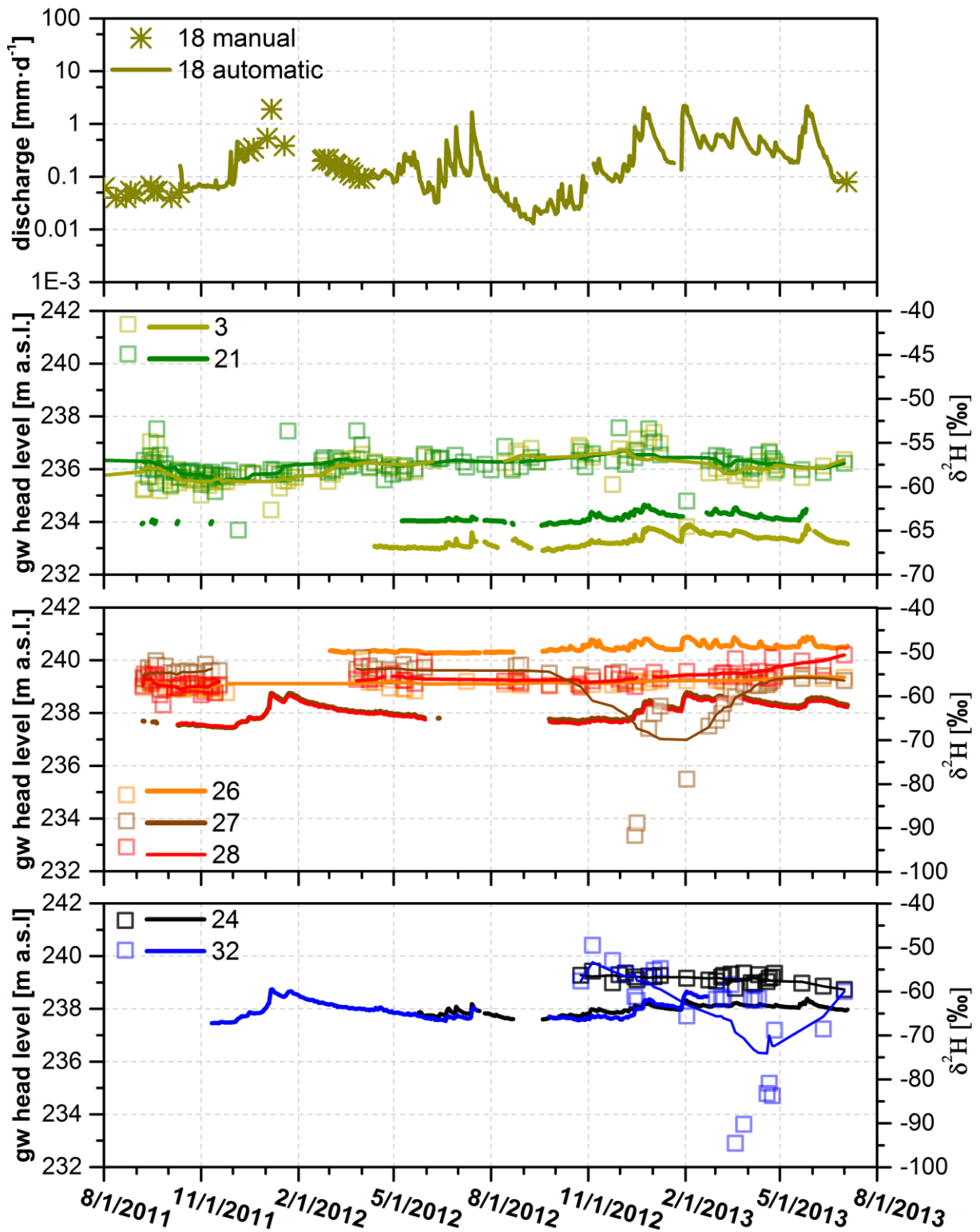
1013

1014 Figure 6. Seasonal $\delta^2\text{H}$ profiles of soil water (upper panels) and water content (lower panels)
 1015 for winter (28 March 2013), summer (28 August 2011), and spring (24 April 2013). Error bars
 1016 represent the natural isotopic variation of the replicates taken during each sampling campaign.
 1017 For reference, mean groundwater (grey shaded) and mean seasonal precipitation $\delta^2\text{H}$ values are
 1018 shown (coloured arrows at the top).



1019
 1020
 1021
 1022
 1023
 1024
 1025
 1026

Figure 7. Mean daily discharge at the Vollnkirchener Bach (13, 18) and Schwingbach (site 11, 19, and 64) with automatically recorded data (solid lines) and manual discharge measurements (asterisks), temporal variation of $\delta^2\text{H}$ of stream water in the Schwingbach (site 11, 19, and 64) and Vollnkirchener Bach (site 13, 18, and 94) including moving averages (MA) for streamflow isotopes.

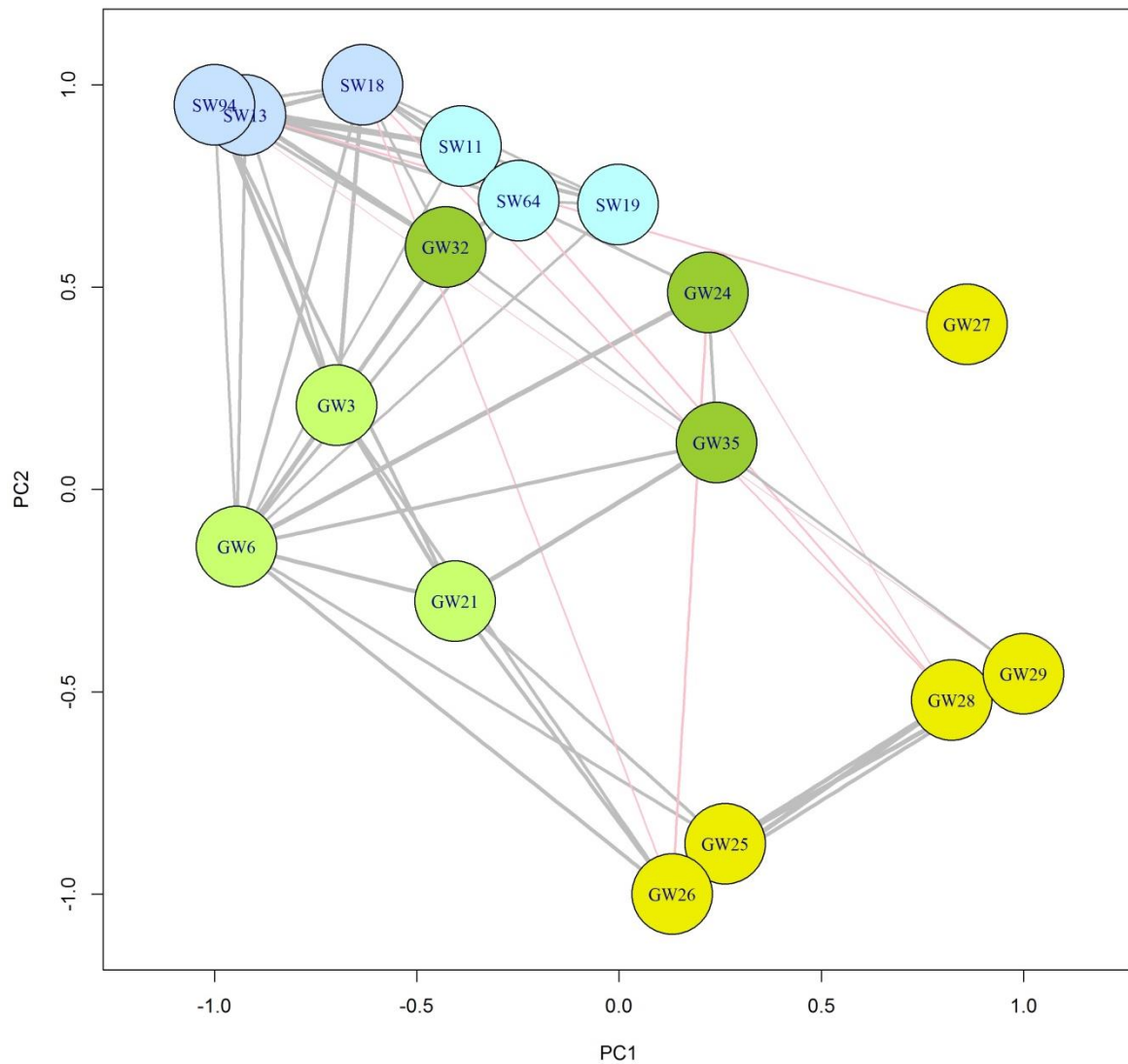


1027

1028

1029 Figure 8. Temporal variation of discharge at the Vollnkirchener Bach with automatically
 1030 recorded data (solid line) and manual discharge measurements (asterisks) (site 18), groundwater
 1031 head levels, and $\delta^2\text{H}$ values (coloured dots) for selected piezometers under meadow (site 3 and

1032 21), arable land (site 26, 27, and 28), and beside the Vollnkirchener Bach (site 24 and 32)
1033 including moving averages for groundwater isotopes.

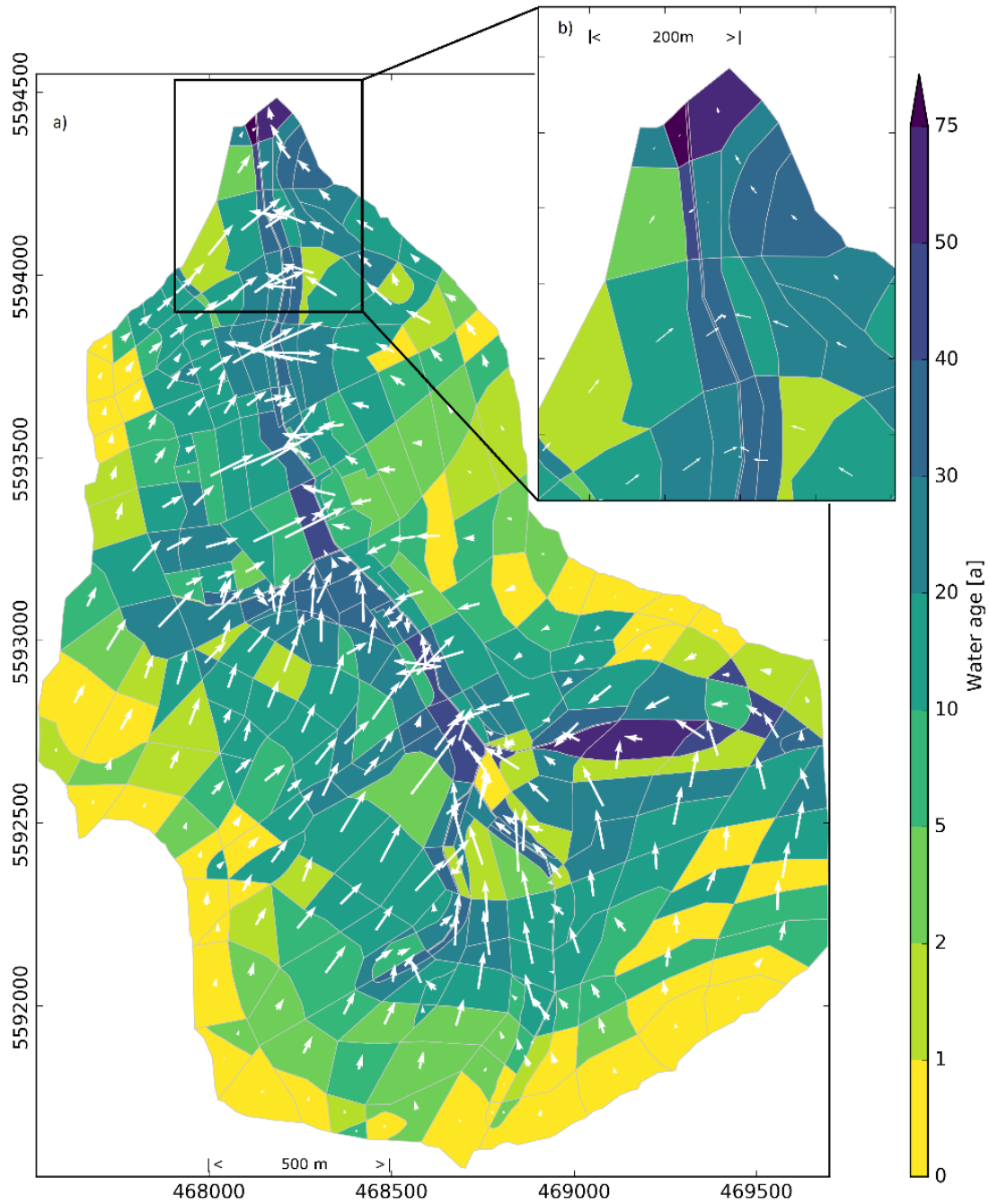


1034

1035

1036 Figure 9. Network map of $\delta^{18}\text{O}$ relationships between surface water (SW) and groundwater
 1037 (GW) sampling points. Yellow circles represent groundwater sampling points on the arable
 1038 field, light green circles are piezometers located on the grassland close to the conjunction of the
 1039 Schwingbach with the Vollnkirchener Bach, and dark green circles represent piezometers along
 1040 the Vollnkirchener Bach. Light blue circles stand for Schwingbach and darker blue circles for
 1041 Vollnkirchener Bach surface water sampling points. See Figure 1 for an overview of all
 1042 sampling points. Only statistically significant connections between $\delta^{18}\text{O}$ time series ($p < 0.05$)
 1043 are shown in the network diagram.

1044



1045

1046

1047 Figure 10. Maps of modelled groundwater ages (colour scheme) and flow directions (white
 1048 arrows) of (a) the Vollnkirchner Bach subcatchment and (b) detail view of the northern part of
 1049 the subcatchment. The length of the white arrows depicts the intensity of flow. UTM-32N
 1050 (WGS84) coordinates on the axis.

1051

1052 **Appendix I**

1053 **Mean transit time estimation**

1054 We applied a set of five different models to estimate the MTT using the FlowPC software
1055 (Maloszewski and Zuber, 2002): dispersion model (with different dispersion parameters
1056 $D_p=0.05, 0.4, \text{ and } 0.8$), exponential model, exponential-piston-flow model, linear model, and
1057 linear-piston-flow model. We evaluated these results using two goodness of fit criteria, i.e.
1058 sigma (σ) and model efficiency (ME) following Maloszewski and Zuber (2002):

$$\sigma = \frac{\sqrt{\sum(c_{mi} - c_{oi})^2}}{m} \quad (1)$$

$$ME = 1 - \frac{\sum(c_{mi} - c_{oi})^2}{\sum(c_{oi} - \bar{c}_o)^2} \quad (2)$$

1059 Where:

- 1060 • c_{mi} : The i-th model result
- 1061 • c_{oi} : The i-th observed result
- 1062 • \bar{c}_o : The arithmetic mean of all observations

1063

1064 A model efficiency $ME=1$ indicates an ideal fit of the model to the concentrations observed,
1065 while $ME=0$ indicates that the model fits the data no better than a horizontal line through the
1066 mean observed concentration (Maloszewski and Zuber, 2002). The same is true for sigma. For
1067 calculations with FlowPC, weekly averages of precipitation and stream water isotopic
1068 signatures are calculated. We firstly calculated the MTT from precipitation to the streams for
1069 three sampling points in the Vollnkirchener Bach (sites 13, 18 and 94) and three points in the
1070 Schwingbach (sites 11, 19 and 64). For the second set of simulations, the mean residence time
1071 from precipitation to groundwater comprising thirteen groundwater sampling points was
1072 determined. We also bias-corrected the precipitation input data with two different approaches:
1073 the mean precipitation value is subtracted from every single precipitation value and then divided
1074 by the standard deviation of precipitation isotopic signatures. Afterwards, this value is
1075 subtracted from the weekly precipitation values (bias1). For the second approach, the difference
1076 of the mean stream water isotopic value and the mean precipitation value is calculated and also
1077 subtracted from the weekly precipitation values (bias2).

1078

1079 **Appendix II**

1080 **Model-based groundwater age dynamics**

1081 Objective:

1082 Stable water isotopes are only a tool to determine the residence time for a few years (McDonnell
1083 et al., 2010). In cases of longer residence times and a strong mixing effect, seasonal variation
1084 of isotopes vanishes and results in barely varying isotopic signals. To get a rough estimate of
1085 residence times greater than the limit of stable water isotopes (>5 years), we split the water flow
1086 path in our catchment in two parts: the flow from precipitation to groundwater, which was
1087 calculated via FlowPC and the longer groundwater transport. The simplest method to estimate
1088 the residence time of groundwater transport is via the storage-to-input-relation, with the storage
1089 as the aquifer size and the input as the groundwater recharge time. However, this method
1090 ignores the topographic setting, and water input heterogeneity. In our study we used a simplified
1091 groundwater flow model with tracer transport to calculate the groundwater age dynamics. The
1092 numerical output of water ages cannot be validated with the given isotope data, since the model
1093 is used to fill a residence time gap, where stable water isotopes are not feasible to apply. The
1094 model is falsified however, if the residence time is short enough (<5 years) to be calculable via
1095 FlowPC. Hence, the results of the groundwater age model should be handled with care and only
1096 seen as the order of magnitude of flow time scales.

1097 Model setup:

1098 We set up a tailored hydrological model for the Vollnkirchener Bach subcatchment using the
1099 *Catchment Modelling Framework* (CMF) by Kraft et al. (2011). CMF is a modular framework
1100 for hydrological modelling based on the concept of finite volume method by Qu and Duffy
1101 (2007). CMF is applicable for simulating one- to three-dimensional water fluxes but also
1102 advective transport of stable water isotopes (^{18}O and ^2H). Thus, it is especially suitable for our
1103 tracer study and can be used to study the origin (Windhorst et al., 2014) and age of water. To
1104 avoid errors in transit time calculations from small differences between the isotopic signal in
1105 groundwater and stream water, we are tracing the transit time of groundwater and not the real
1106 isotopic values in this study. The generated model is a highly simplified representation of the
1107 Vollnkirchener Bach subcatchment's groundwater body. The subcatchment is divided into 353
1108 polygonal-shaped cells ranging from 100–40'000 m² in size based on land use, soil type, and
1109 topography. The model is vertically divided in two compartments, the upper soft rock aquifer,
1110 and the lower bed rock aquifer, referred to as upper and lower layer from now onwards.

1111 The layers of each cell are connected using a mass conservative Darcy approach with a finite
 1112 volume discretization. The water storage dynamic of one layer in one cell i of the groundwater
 1113 model is given as:

$$\frac{dV_{i,s}}{dt} = R_i - S_i - \sum_{j=1}^{N_i} \left(K_s \frac{\Psi_{i,s} - \Psi_{j,s}}{d_{ij}} A_{ij,s} \right) \quad (3)$$

$$\frac{dV_{i,b}}{dt} = S_i - \sum_{j=1}^{N_i} \left(K_b \frac{\Psi_{i,b} - \Psi_{j,b}}{d_{ij}} A_{ij,b} \right)$$

1114

1115 Where:

- 1116 • V_i : The water volume stored by the layer in m^3 in cell I for soft rock (s) and bedrock
 1117 (b), respectively
- 1118 • R_i : The groundwater recharge rate in $\text{m}^3 \cdot \text{d}^{-1}$
- 1119 • S_i : the percolation from the soft rock to the bedrock aquifer, calculated by the
 1120 gradient and geometric mean conductivity between the layers: $S_i =$
 1121 $\sqrt{K_s K_b} \frac{\Psi_{i,s} - \Psi_{i,b}}{d_{sb}} A_i$, where d_{sb} is the distance between the layers and A_i is the cell area
- 1122 • N_i : Number of adjacent cells to cell i
- 1123 • K : Saturated hydraulic conductivity in $\text{m} \cdot \text{d}^{-1}$ for soft rock (s) and bedrock (b),
 1124 respectively
- 1125 • Ψ : Water head in the current cell i and the neighbour cell j in m for soft rock (s) and
 1126 bedrock (b), respectively
- 1127 • d_{ij} : The distance between the current cell i and the neighbour cell j in m
- 1128 • $A_{i,j,x}$: The wetted area of the joint layer boundary in m^2 between cells i and j in layer
 1129 x

1130 The volume head relation is linearized as $\Psi = \phi \frac{V}{A}$, with ϕ being the fillable porosity and A the
 1131 cell area. The resulting ordinary differential equation system is integrated using the CVODE
 1132 solver by Hindmarsh et al. (2005), an error controlled Krylov-Newton multistep implicit solver
 1133 with an adaptive order of 1–5 according to stability constraints.

1134 Boundary conditions:

1135 The upper boundary condition of the groundwater system – the mean groundwater recharge –
1136 is modelled applying a Richard's equation based model using measured rainfall data (2011–
1137 2013) and calculated evapotranspiration with the Shuttleworth-Wallace method (Shuttleworth
1138 and Wallace, 1985) including land cover and climate data. To retrieve long-term steady state
1139 conditions, the groundwater recharge is averaged and used as constant flow Neumann boundary
1140 condition. The total outflow is calibrated against measured outflow data; hence, the unsaturated
1141 model's role is mainly to account for spatial heterogeneity of groundwater recharge. As an
1142 additional input, a combined sewer overflow (site 38, Fig. 1b) is considered based on findings
1143 of Orłowski et al. (2014). Moreover, there are two water outlets in the two lowest cells for
1144 efficient draining, reflecting measured groundwater flow directions throughout most of the year
1145 at piezometers 1–6 (Fig. 1b). Both cells are located in the very north of the subcatchment and
1146 their outlets are modelled as constant head Dirichlet boundary condition.

1147 Parameters:

1148 The saturated hydraulic conductivity of the groundwater body is set to 0.1007 m d^{-1} , as
1149 measured in the study area. For the lower bedrock compartment there is no data available.
1150 However, expecting a high rate of joints, preliminary testing revealed that a saturated hydraulic
1151 conductivity of 0.25 m d^{-1} seemed to be a realistic estimation (based on field measurements).

1152 Water Age:

1153 To calculate the water age in each cell, a virtual tracer flows through the system using advective
1154 transport. To calculate the water age from the tracer that enters the system with a unity
1155 concentration by groundwater recharge, a linear decay is used to reduce the tracer concentration
1156 with time:

$$\frac{dX_{i,s}}{dt} = 1 \frac{u}{m^3} R_i - S_i [X]_{i,s} - \sum_{j=1}^{N_i} \left([X]_{i,s} K_s \frac{\Psi_{i,s} - \Psi_{j,s}}{d_{ij}} A_{ij,s} \right) - r X_{i,s} \quad (4)$$
$$\frac{dX_{i,b}}{dt} = S_i [X]_{i,s} - \sum_{j=1}^{N_i} \left([X]_{i,b} K_b \frac{\Psi_{i,b} - \Psi_{j,b}}{d_{ij}} A_{ij,b} \right) - r X_{i,b}$$

$$t_{ix} = \frac{\ln[X]_{ix}}{r}$$

1157

1158 Where:

- 1159 • $X_{i,x}$: Amount of virtual tracer in layer x in cell i in virtual unit u
- 1160 • $1 \frac{u}{m^3} R_i$: Tracer input with groundwater recharge R with unity concentration
- 1161 • $[X]_{i,x}$: Concentration of tracer in layer x of cell i in $u m^{-3}$
- 1162 • r : Arbitrary chosen decay constant, for water age calculation in d^{-1} . Rounding errors
- 1163 occur due to low concentrations when r is set to a high value. We found a good
- 1164 numerical performance with values between 10^{-6} – $10^{-9} d^{-1}$
- 1165 • t_{ix} : Water age in days in layer x in cell i

1166

1167 To ensure long term steady state conditions, the model is run for 2000 years. However, after
1168 300 years of model run time, steady state is reached.